Displaced Fock States and Photon Correlations in Glauber-Fock Photonic Lattices

by

Armando Pérez Leija

A dissertation submitted in partial fulfillment of

the requirements for the **degree of**

Doctor of Philosophy in the National Institute

for Astrophysics, Optics, and

Electronics, INAOE

Tonantzintla, Puebla, México

Advisor:

Dr. Héctor Manuel Moya Cessa

25th August 2011

Abstract

Light propagation in waveguide lattices has been the subject of considerable interest during the last few years. Such array structures provide a versatile platform upon which one can observe a host of processes, such as optical Bloch oscillations, Zener tunneling, Rabi oscillations, Talbot revivals, and discrete solitons, to mention a few [1, 58, 40, 12]. The discrete diffraction properties of such configurations can mold the flow of light in a predictable manner, hence providing altogether new opportunities for applications. Quite recently light propagation in random and quasi-random arrays has also been considered-ranging from ballistic to the Anderson localization regime [49, 12]. In addition, quantum correlations in regular lattice structures have been investigated for both classical and completely quantum states [28]. Yet, despite of all the efforts put in this area, only a few of the reported lattices are known to have closed form solutions [26, 58]. In fact, integrable discrete systems are rather rare and any new addition to this class will further facilitate such fundamental studies.

In the present work we introduce two new types of integrable photonic lattices exhibiting new families of physical processes like those occurring in quantum optics.

We predict the emergence of classical analogues to coherent and displaced quantum states. These classical *states* arise as the impulse response of Glauber-Fock photonic lattices [40], whose inter-channel coupling constants obey a square root law. In addition, we provide the first observation of classical intensity distributions in optical arrays that are totally analogous to quantum coherent and displaced Fock states. Bloch-like oscillations and revivals are also predicted in such Glauber-Fock photonic lattices. Special consideration is devoted to describe quantum correlations of single photon and path entangled states propagating in these novel integrated optical structures. In summary, we realized a Glauber-Fock photonic lattice to directly observe an optical analogue for the displacement of Fock states and investigated a new family of photon correlations occurring in this optical system.

Contents

List of Figures

Dedicated to Sayde and Zyanya

Acknowledgements

First of all, I would like to thank the great people of México for giving me the opportunity to study all the way from the primary school through the PhD in public schools. Because thanks to them all the Mexican public institutions exist and they give life to many dreams and realities.

I am grateful to my parents for all their guidance and support during all the stages of my life. Having them as a life-advisors was really an invaluable support. I would like to thank my advisor, Professor Héctor Manuel Moya Cessa, for his teaching, overall support, guidance, freedom, and patience all these years.

I need to thank Professor Demetrios Christodoulides for giving me the opportunity and freedom to work with him in CREOL, the College of Optics and Photonics at the University of Central Florida. A great part of the work presented in this thesis would not have been possible without his help.

Last, but certainly not least, I would like express my gratitude and love to Sayde Alcántara Santiago. Her unconditional support, and encouragement gives me the strength and will to never quit and to always do the best through this long journey.

She has always taught me to cherish life and to keep my feet grounded. She is, and always will be, my foundations and reasons.

Chapter 1

Introduction

During the last decades, the ability to mold and engineer the flow of classical and non-classical light in order to perform intelligent all-optical functions has become an important topic in science and technological applications [1]. For instance, completely optical networks make possible to leave aside the relatively slow electronic devices in favor of optical switches and logic gates taking full advantage of the bandwidth capabilities of optical fibers; thus significantly increasing the speed of communication systems. On the other hand, the processing of information encoded in quantum systems admitting quantum superpositions and entanglement provides exponentially greater power for particular tasks such as quantum factoring algorithms and the simulation of complex quantum systems [2]. In fact, a wide variety of quantum circuits have so far been realized for quantum metrology, lithography, quantum logical gates, and another entangling circuits [3]. Despite the progress

reached along those lines, the aforementioned applications have been implemented and demonstrated using bulk optical elements (beam splitters, phase shifters, etc). As might be expected, these approaches exhibit several intrinsic disadvantages like being bolted to large optical tables making them inherently unscalable. Quite recently, however, the exquisite control achieved in state-of-the-art micro-fabrication now enables studying the propagation of quantum states of light, such as single photon and correlated photon states, in a new classes of photonic circuits based on integrated optical systems [4]. The advantages presented by integrated photonic systems include miniaturization, robustness, scalability, and high fidelity, to mention a few [4, 5, 6]. One of the most basic integrated devices are the so-called directional couplers, which are formed when two optical waveguides are placed in close proximity of each other so that the optical tunneling is easily achieved. Even though, the number of ports provided by directional couplers can in principle be expanded via cascading, the implementation of N by N port systems becomes increasingly difficult as the number of nodes increases. Of importance is to devise a new generation of N by N port systems capable of routing and processing a variety of quantum states. Arrays of optical waveguides may very while be a prime candidate for achieving such operations [7]. The discrete nature of these array structures implies certain versatility that has been exploited by several groups around the world to optically mimic a huge platform of physical processes [8, 9, 10, 11, 12, 13, 14]. For example, optical waves propagating in lattices of equally spaced identical waveguides encounter a

periodic spatial change in the refractive index profile. To the light, this refractive index distribution behaves as a periodic potential, thus optical waves propagating in such a structure behave in a manner that is analogous to electrons traveling through semiconductor crystals. As a direct result of their periodic nature, these array structures possess all of the fundamental characteristics of a crystalline lattice such as allowed and forbidden bands. In addition, since light is confined within individual waveguides, the optical field can be viewed as the superposition of a finite set of bound modes each having its own unique propagation constant and modal profile. Although the modal profiles themselves are continuous, the over-all propagation dynamics can be approximated by considering only the amplitude and phase of the mode. Consequently, the wave propagation is effectively discretized, and the underlying field evolution exhibits behavior characteristic of discrete systems [1].

Therefore, through the process of optical tunneling, light propagating in waveguide arrays is transported from one waveguide site to adjacent waveguide sites. This profoundly alters the overall diffraction behavior along the system yielding to the so-called discrete diffraction process. In one-dimensional (1D) waveguide arrays, discrete diffraction, was first addressed theoretically by Alan L. Jones in 1965 [15] and was experimentally observed in waveguide arrays fabricated in gallium arsenide (GaAs) a few years later [16]. However, at that time it was not obvious how one could take advantage of or suppress this diffraction process, therefore the field remained dormant for many years.

The study of systems of coupled waveguides was resumed in 1988, when Christodoulides and Joseph suggested the idea that light could self-localize in nonlinear optical waveguide arrays [17]. As a consequence, new areas of study in classical optics came along, among them the discovery of optical discrete solitons, Bragg and vector solitons in fiber arrays, discrete nonlinear surface waves, etc, [18]. Thereafter, in 1991, Lai, Buzek, and Knight established the theory for non-classical light propagating through linear directional couplers [19]. Since then a growing interest in the study of propagation of nonclassical light in coupled waveguides has been arisen in the scientific community. From the technological point of view, perhaps the most remarkable example is the realization of quantum C-Not gates using sets of directional couplers [2]. In this particular example, a set of bulk optical devices, beam splitters, were replaced by directional couplers obtaining the first integrated quantum circuit.

Besides applications to conventional quantum computers, multipartite quantum states have emerged as a crucial resource for new directions in quantum information processing such as measurement-based on quantum computation, quantum secret sharing, and quantum simulation. It is thus important to understand the behavior of single photons and more generally nonclassical light in integrated optical systems [20].

The main goal of the work presented in this dissertation is to provide new additions to integrable photonic lattices exhibiting new families of physical processes

like those occurring in quantum optics. Special consideration is devoted to describe quantum correlations of single photon and entangled states propagating in these novel integrated optical structures.

In Chapter 2 we give a brief review of the basic theory of the underlying physics necessary to understand wave propagation in linear discrete optical systems. Coupled mode theory is presented and used to find a discrete model for the evolution of the modal electric fields in directional couplers. Then, the extension to systems involving more than two waveguides, waveguide arrays, is discussed in some detail. Finally, having established the standard classical coupled-mode equations we turn to the quantum-mechanical description of the same systems. It is shown that a directional coupler follows the same dynamics of beam splitter with reflection and transmission coefficients varying continuously along the propagation distance.

The realization of classical analogs to quantum coherent and displaced Fock states in one-dimensional semiinfinite photonic lattices having a square root law for the coupling coefficients are theoretically predicted in Chapter 3. Beam dynamics in these fully integrable structures is described in closed form, irrespective of the site of excitation. The trajectories of these beams are closely examined, and pertinent examples are provided for their realization. Following these theoretical results, the second section on this chapter deals with a detailed explanation of the experimental realization of these classical states.

In Chapter 4 we analyze the correlations for pairs of separable and path-entangled

photons as well as of (notional) fermions in Glauber-Fock lattices. It is shown how their correlation patterns uniquely depend on the input position as is expected from the inherent broken symmetry of these particular lattices.

Chapter 5 focuses on the theoretical prospect of classically emulate a driven quantum harmonic oscillator via sinusoidally curved photonic lattices. Wave propagation dynamics is given in close form and numerical simulations are achieved to corroborate our theory. Interestingly these lattices exhibit Bloch-like oscillation even though they are not periodic. In addition, a resonant condition for dynamic localization is provided.

The main results and conclusions of this dissertation are presented in the final Chapter 6.

Chapter 2

Linear waveguide arrays

The main goal of this chapter is to provide a basic review of how optical beams propagate through infinite waveguide arrays. In order to understand optical wave dynamics in such arrays it is necessary to first consider the theory of electromagnetic wave propagation in linear directional couplers. Then, from this model we can easily infer the equations governing light evolution through linear structures involving more than two waveguides.

The propagation of electromagnetic waves in a single optical waveguide can be solved exactly by application of Maxwell equations [21]. This is not the case, however, in a two waveguide-structure: the so-called directional coupler. To describe light propagation through such a system one must to resort on perturbation methods. One such method is the so-called *coupled mode theory*, which was first developed by Pierce to treat the coupling between electron beam waves, and later extended

to optical waveguides by Marcuse [22] and many others [23]. In this approach one assumes that the presence of one waveguide introduces a small perturbation in the other waveguide. The electric (or magnetic) field of the composite structure may then be taken as a linear superposition of the unperturbed fields of each waveguide in isolation. If one then substitutes this into the Maxwell equations, it yields to two first order differential equation in the slow varying envelope approximation for the amplitudes of the fields in each guide, and these may be readily solved. One of the main predictions of the coupled-mode theory is the way in which energy can be transferred from one waveguide to the other in a controlled fashion [24], providing altogether new opportunities for applications.

2.1 Classical coupled mode-equations

An optical waveguide consist in its simplest form of a central core with a refractive index higher than the surrounding cladding material.The modes which propagate unattenuated along the waveguide are known as guided modes [22], as opposed to the radiation modes which radiate away. In a translational waveguide, the guided modes are expressible in the separable form

$$E(x, y, z, t) = E_m(x, y)e^{i(\omega t - \beta_m)}, \tag{2.1}$$

where $E_m(x, y)$ is the transverse mode pattern, β_m is the associated propagation

constant, and ω is the frequency [25]. We have assumed for simplicity that the field are linearly polarized. For the linear directional coupler, we do not require explicit forms for the mode patterns. Each guided mode is a solution of the wave equation

$$\left[\nabla_t^2 + \frac{\omega^2 n^2}{c^2} - \beta_m^2\right] E_m = 0, \tag{2.2}$$

where ∇_t^2 is the transverse Laplacian operator. For the step-index profile waveguide, Eq.(2.2) must hold in each region of the guide and the fields matched at the core-cladding interface. It is well known that the orthogonality of the guided modes is mathematically given by:

$$\int E_m^*(x,y) E_n(x,y) dxdy = \frac{2\omega\mu_0}{|\beta_m|}\delta_{nm}, \tag{2.3}$$

where it has been assumed the modes are normalized such that one unit of energy flows through the cross section of the waveguide.

A schematic arrangement of a directional coupler is shown in Fig.2.1. Each waveguide in isolation is assumed to support one guided mode E_i $(i = 1, 2)$ with propagation constant β_i satisfying the wave equation

$$\left[\nabla_t^2 + \frac{\omega^2 n^2}{c^2} - \beta_i^2\right] E_i = 0, \qquad i = 1, 2. \tag{2.4}$$

In the framework of coupled mode theory, the electric (or magnetic) field of the composite structure is assumed to be a linear superposition of the unperturbed fields

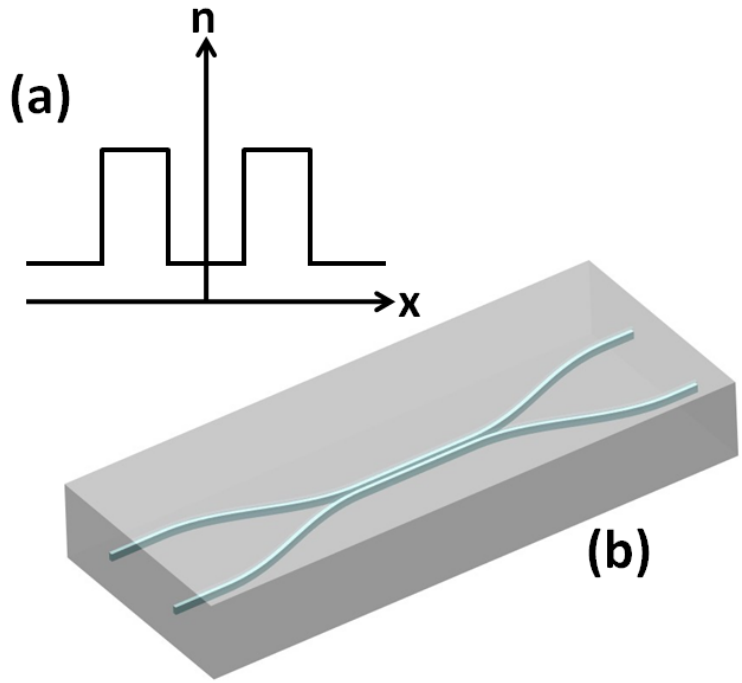

Figure 2.1: **Schematic illustration of a linear directional coupler having two waveguides and rectangular cross sections. Fig.(a) Depicts the refractive index profile along x.**

$$E(x,y,z,t) = a_1(z)E_1(x,y)e^{i(\omega t-\beta_1 z)} + a_2(z)E_2(x,y)e^{i(\omega t-\beta_2 z)}, \tag{2.5}$$

where $a_{1,2}(z)$ are the slowly varying functions of z. When the waveguides are placed sufficiently far apart, $a_1(z)$ and $a_2(z)$ are independent of z. In other words, when the waveguides are far away each from the other such that the corresponding propagating fields do not interact, the field amplitudes travel invariantly along z. Substituting Eq.(2.5) into the wave equation

$$\left[\nabla^2 + \frac{\omega^2 n^2}{c^2}\right] E = 0, \tag{2.6}$$

making the slowly varying amplitude approximation, and using the normalization condition (2.3),

$$\begin{aligned} i\frac{da_1}{dz} &= -(\Delta\beta_1)a_1 - (\kappa_{1,2})a_2 e^{i(\beta_1-\beta_2)z}, \\ i\frac{da_2}{dz} &= -(\Delta\beta_2)a_2 - (\kappa_{1,2})a_1 e^{i(\beta_1-\beta_2)z}, \end{aligned} \tag{2.7}$$

where

$$\begin{aligned} \Delta\beta_i &= \frac{4\epsilon_0}{4}\int\int \left(n_i^2 - n_{cl}^2\right) E_j^* E_j dxdy, \qquad i \neq j \\ \kappa_{i,j} &= \frac{4\epsilon_0}{4}\int\int \left(n_i^2 - n_{cl}^2\right) E_i^* E_j dxdy, \qquad i \neq j. \end{aligned} \tag{2.8}$$

The elements $\Delta\beta_i$ are small corrections to the propagation constants and arise due to the presence of the field propagating through the adjacent waveguide [25]. Whereas the elements $\kappa_{i,j}$ $(i \neq j)$ represent the coupling between the modes of the two waveguides. By assuming identical waveguides, $(\beta_1 = \beta_2 = \beta)\,, and\,(\kappa_{1,2} = \kappa_{2,1} = \kappa)$, Eq.(2.7) can be written as

$$i\frac{da_1}{dz} = -\Delta\beta a_1 - \kappa a_2,$$
$$i\frac{da_2}{dz} = -\Delta\beta a_2 - \kappa a_1, \tag{2.9}$$

In matrix form we have

$$i\frac{d}{dz}\begin{pmatrix} a_1 \\ a_2 \end{pmatrix} = -\begin{pmatrix} \Delta\beta & \kappa \\ \kappa & \Delta\beta \end{pmatrix}\begin{pmatrix} a_1 \\ a_2 \end{pmatrix} \tag{2.10}$$

Equation (2.10) can be readily solved by calculating the exponential of the coupling matrix, then by doing so we obtain

$$\begin{pmatrix} a_1(Z) \\ a_2(Z) \end{pmatrix} = \exp(-i\Delta\beta Z)\begin{pmatrix} \cos(\kappa Z) & -i\sin(\kappa Z) \\ -i\sin(\kappa Z) & \cos(\kappa Z) \end{pmatrix}\begin{pmatrix} a_1(0) \\ a_2(0) \end{pmatrix} \tag{2.11}$$

When waveguide $a_1(Z)$ is excited, $a_1(Z) = 1$, $a_2(Z) = 0$, then the solution is simply

$$a_1(Z) = \cos(\kappa Z)$$
$$a_2(Z) = i\sin(\kappa Z) \tag{2.12}$$

The intensity distribution is displayed in Fig.2.2. As light propagates along the waveguides, the energy is completely coupled to the adjacent channel as predicted by Eqs.(2.12). A very useful parameter is the coupling length, defining the propagation

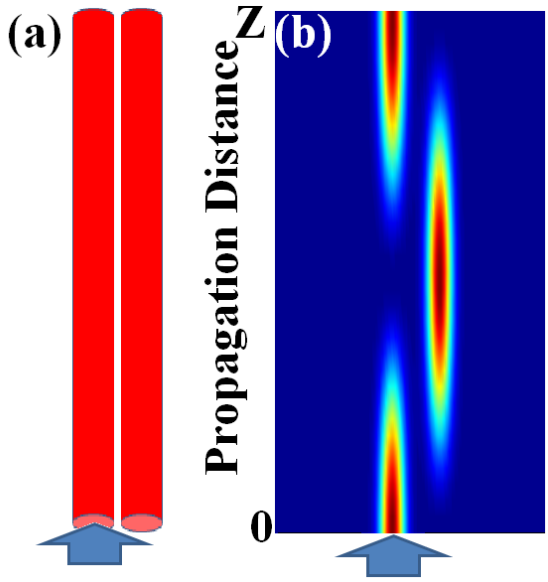

Figure 2.2: **(a) Schematic view of the simulated linear directional coupler. (b) Intensity evolution when light is injected into the left waveguide. The arrow indicates the input beam.**

distance l_c after which in a two waveguide system all of the guided power in the excited waveguide has been coupled in the adjacent one. In this case, it follows from Eq.(2.12) that $\cos(\kappa l_c) = 0$ yields to the coupling length $l_c = \pi/2\kappa$.

The preceding discussion assumes that only two waveguides are involved in the coupling, but coupled mode theory can also be applied to problems involving more than two waveguides [1]. In the case of an infinite array of identical and equally spaced waveguides, the coupled mode relations are

$$i\frac{dE_n}{dz} + \Delta\beta E_n + \kappa\left(E_{n+1} + E_{n-1}\right) = 0, \qquad \forall \qquad n \tag{2.13}$$

where E_n, as before, is the modal electric field in the $n\text{-}th$ waveguide, $\Delta\beta$ is the correction to the propagation constants, and κ the coupling coefficients. In order to study the diffraction properties for this infinite waveguide array it is first important to derive its impulse response,i.e., when only one single channel is excited. Then, the infinite set of ordinary differential equations is analytically integrable in terms of Bessel functions of the first kind [26]. If we set $E_n(0) = 1$, the solution for the light evolution in the $n - th$ waveguide is

$$E_n(Z) = (i)^n \exp(-i\beta Z) J_n(2\kappa Z) \tag{2.14}$$

This distribution is displayed in Fig. 2.3. As the light propagates along the waveguides, the energy spreads into two main lobes with several secondary peaks between them. The solution under any other initial conditions will be a linear superposition of Eq. (2.14).

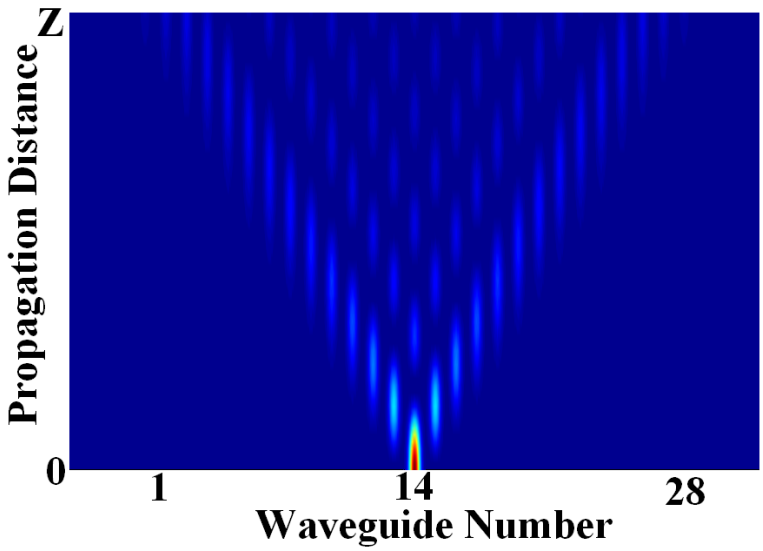

Figure 2.3: **Solution for a linearly coupled array of 30 waveguides when light is injected into the central channel with an amplitude $E_{14}(0) = 1$. The energy spreads mainly into two lobes, i.e., in such an array, light will couple to more and more waveguides as it propagates, thereby broadening its spatial distribution. This widening distribution is analogous to diffraction in continuous media.**

2.2 Operator coupled mode-equations and quantum correlations

Having established the standard classical coupled mode equations we now turn to the quantum mechanical description of coupled waveguides. The quantization for a directional coupler is straightforward if we consider that the coupler is made of

identical optical waveguides each supporting a single transverse mode. Then, by establishing a correspondence between the mode amplitudes and the amplitudes of two linearly coupled harmonic oscillators with a Hamiltonian [27]

$$H = \Delta\beta\left(a_1^\dagger a_1 + a_2^\dagger a_2\right) + \kappa\left(a_1^\dagger a_2 + a_2^\dagger a_1\right), \tag{2.15}$$

we can find the evolution of the quantized electromagnetic field in each waveguide given by [19]

$$\begin{aligned} i\frac{da_1^\dagger}{dZ} &= -[a_1^\dagger, H] = \Delta\beta a_1^\dagger + \kappa a_2^\dagger \\ i\frac{da_2^\dagger}{dZ} &= -[a_2^\dagger, H] = \Delta\beta a_2^\dagger + \kappa a_1^\dagger \end{aligned} \tag{2.16}$$

The creation operators at any distance along propagation are calculated by integrating Eq.(2.16)

$$\begin{pmatrix} a_1^\dagger(Z) \\ a_2^\dagger(Z) \end{pmatrix} = \exp(i\Delta\beta Z) \begin{pmatrix} \cos(\kappa Z) & -i\sin(\kappa Z) \\ -i\sin(\kappa Z) & \cos(\kappa Z) \end{pmatrix} \begin{pmatrix} a_1^\dagger(0) \\ a_2^\dagger(0) \end{pmatrix} \tag{2.17}$$

From Eq.(2.17) it is obvious that $\exp(i\Delta\beta Z)$ is just a global phase factor, therefore it is unphysical and can be neglected. Actually this phase factor arose from the consideration of the individual field energies in the Hamiltonian. Therefore, we lose no generality by leaving them off of consideration in the Hamiltonian.

$$H = \kappa\left(a_1^\dagger a_2 + a_2^\dagger a_1\right), \tag{2.18}$$

From this discussion it is obvious that a directional coupler acts exactly as a beam splitter, with the reflection and transmission coefficients varying continuously along the propagation. If two photons were injected into the coupler, one to each waveguide, the average photon number in each waveguide is constant since

$$n_{1(2)} = \langle a^{\dagger}_{1(2)} a_{1,(2)} \rangle = \cos^2(\kappa Z) + \sin^2(\kappa Z) = 1. \tag{2.19}$$

It means that the probability distribution of a single photon evolves in the same way as the intensity distribution of classical light. Therefore, measurements of the probability distribution for single photons are not enough to reveal the quantum properties of light [28]. However, insight into quantum effects can be obtained by regarding the photon number correlation function. As an example consider two photons simultaneously launched into the input ports of a coupler, $|\psi\rangle_{input} = |1\rangle_1 |1\rangle_2$, so that the probability to detect exactly one photon at each waveguide (a coincidence measurement) is given by the correlation function

$$\Gamma_{1,2}(Z) = \langle a^{\dagger}_1 a^{\dagger}_2 a_2 a_1 \rangle = |\cos^2(\kappa Z) - \sin^2(\kappa Z)|^2 = \cos^2(2\kappa Z) \tag{2.20}$$

Therefore, since two paths lead to the final state of one photon at each waveguide, they interfere and the probability for a coincidence measurement oscillates along propagation. Note that after propagating exactly half a coupling length $Z = \pi/4\kappa$ the photon number correlation function is zero. At this point both photons are

found traveling together in the same waveguide but we have no knowledge of which waveguide is that. This result is analogous to the well known experiment carried out by Hong, Ou, and Mandel by using a beam splitter in 1987 [29]. Then, because of the interplay of single photons traveling through systems of coupled waveguides is equivalent to the dynamical processes occurring in beam splitters, we can conclude that it is possible to cascade several of them in order to implement quantum gates in an integrated manner. A lattice of many coupled waveguides enriches the variety of correlations obtained in integrated structures, as we show bellow.

We now turn to study the quantum properties of a periodic lattice with a large number of identical waveguides, with equal coupling constants. The evolution of the quantized electromagnetic field in each waveguide is inferred from the Heisenberg equation for the bosonic creation operators of a coupler. Thus, the set of Heisenberg equations for the creation operators is given by

$$i\frac{d}{dZ}\begin{pmatrix} \vdots \\ a^{\dagger}_{n-1} \\ a^{\dagger}_{n} \\ a^{\dagger}_{n+1} \\ \vdots \end{pmatrix} = \begin{pmatrix} \dots & \vdots & \vdots & \vdots & \vdots & \vdots & \dots \\ \dots & \kappa & \Delta\beta & \kappa & 0 & 0 & \dots \\ \dots & 0 & \kappa & \Delta\beta & \kappa & 0 & \dots \\ \dots & 0 & 0 & \kappa & \Delta\beta & \kappa & \dots \\ \dots & \vdots & \vdots & \vdots & \vdots & \vdots & \dots \end{pmatrix} \begin{pmatrix} \vdots \\ a^{\dagger}_{n-2} \\ a^{\dagger}_{n-1} \\ a^{\dagger}_{n} \\ \vdots \end{pmatrix}$$

Throughout we will use the following short expression to represent this set of differential equations

$$i\frac{da_n^\dagger}{dZ} = \Delta\beta a_n^\dagger + \kappa\left(a_{n+1}^\dagger + a_{n-1}^\dagger\right). \tag{2.21}$$

Thus, the unitary transformation between input and output states becomes

$$a_n^\dagger(Z) = \exp(i\Delta\beta Z)\sum_{q=0}^{\infty} E_{n,q}(Z)a_q^\dagger(Z=0), \tag{2.22}$$

where $E_{n,q}(Z) = [\exp(iMZ)]_{n,q}$, and M is defined as

$$M = \begin{pmatrix} \dots & \vdots & \vdots & \vdots & \vdots & \vdots & \dots \\ \dots & \kappa & \Delta\beta & \kappa & 0 & 0 & \dots \\ \dots & 0 & \kappa & \Delta\beta & \kappa & 0 & \dots \\ \dots & 0 & 0 & \kappa & \Delta\beta & \kappa & \dots \\ \dots & \vdots & \vdots & \vdots & \vdots & \vdots & \dots \end{pmatrix}$$

The term $E_{n,q}(Z)$ in Eq.(2.22) represents the n-*th* row of the q-*th* column within the exponential of the coupling matrix. At this point, perhaps is beneficial to clarify that in order to obtain analytical expressions for light evolution through these arrays, the number of waveguides is considered infinite. On the other hand, from the practical point of view, such solutions can effectively be observed by launching light into the central channels avoiding reaching the boundaries.

As in the two waveguide case, when single photons are coupled into the array,

they will evolve following the classical intensity distributions. When a single photon is launched into the k-*th* site, the probability to find it at waveguide m-*th* after propagating a distance Z is given by the average photon number at waveguide m

$$n_m = |E_{m,k}(Z)|^2 = [J_{q,k}(2\kappa Z)]^2, \tag{2.23}$$

$E_{m,k}(Z)$ is the m-*th* element of the k-*th* row within the unitary transformation, and J_q is the q-*th* Bessel function of the first kind. Because Eq.(2.23) gives the same distribution that classical light evolution through the same array, provided a correspondence probability $\rightarrow$ classical intensity, the photon spreads across the lattice by coupling from one waveguide to its neighbors describing a pattern characterized by two strong lobes as it was shown in Fig.2.3 for classical light. If a second photon is coupled to another waveguide l, then the average photon number at waveguide m is simply the incoherent superposition

$$n_m = \langle a_m^\dagger a_m \rangle = |E_{m,k}(Z)|^2 + |E_{m,l}(Z)|^2 = [J_{q,k}(2\kappa Z)]^2 + [J_{q,l}(2\kappa Z)]^2. \tag{2.24}$$

Therefore, once again the quantum nature of light is unveiled by considering the correlations between the two photons. In what follows we study the correlation matrix, $\Gamma_{p,q}$, for three distinct two photon input state configurations. Such a correlation matrix, $\Gamma_{p,q}$, provides the probability map of detecting one photon at waveguide p and its twin at waveguide q.

Case one: Separable single photon input states.

1-A) Both photons are coupled to a single waveguide at the center of the lattice.

1-B) The two photons are coupled to two adjacent waveguides.

1-C) The two photons are coupled to two waveguides separated by one waveguide.

Case two: Path entangled pair of photons.

2-A) Path-entangled pair of photons in adjacent waveguides.

Case three: Pair of photons in the quantum lithography scheme.

3-A) Path-entangled pair of photons with correlated positions.

3-B) Path-entangled pair of photons with anti-correlated positions.

All these input states can be experimentally realized by coupling spontaneously down-converted photons into the lattice. Then, by carefully designing the phase matching conditions and the collecting optics, the down-converted photons can be directed to yield the desired input configuration.

2.2.1 Case 1: Separable single photon input states.

1-A) Both photons are simultaneously coupled into the central waveguide of the array, i.e., at the zeroth channel.

Since a single photon being launched into the p-*th* waveguide can be represented via the creation operators $a_p^\dagger$ and the vacuum state $|0\rangle$, the present input state can be written as

$$|\psi_0\rangle = \frac{1}{\sqrt{2}}\left[a_0^\dagger\right]^2 |0\rangle\,. \tag{2.25}$$

In this case, the correlation matrix, $\Gamma_{p,q} = 2|E_{p,0}E_{q,0}|^2$, does not exhibit any type of quantum interference, it is just the product of two probability distributions. Figures 2.4(a, b) show the photon density evolution for a regular array containing sixty elements, and the probability distribution at the output after propagating a normalized distance $Z = 12$, respectively. Figures 2.5(b, c) depict the correlation matrix when both photons are coupled into the zeroth channel at the center of the array. The correlation map is characterized by four strong lobes at the corners of the matrix, resulting from the tendency of the photons to propagate to the neighborhood of the dominant lobes (see Figs.2.4(a, b)).

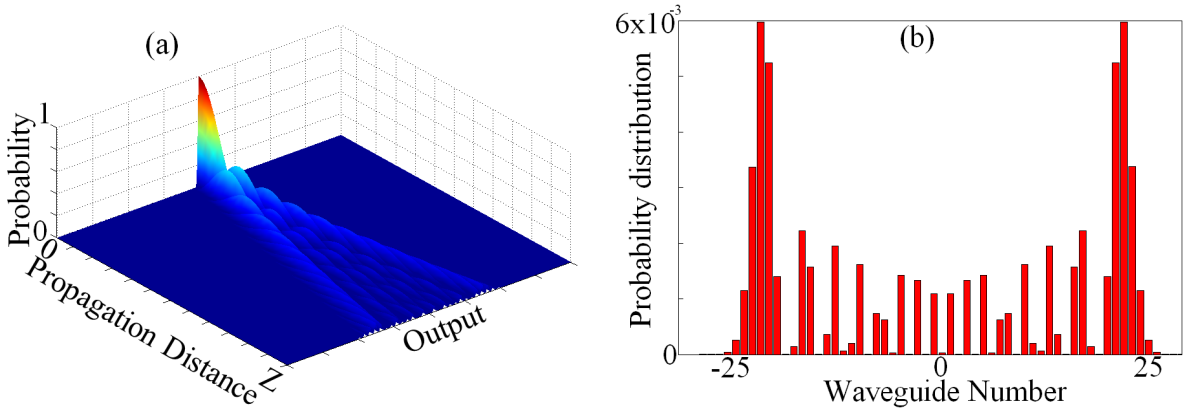

Figure 2.4: **(a) Evolution of the probability distribution along propagation for a single photon injected into the central channel of the lattice. (b) Probability distribution at the output (normalized distance $Z = 12$)**

1-B) The photons are simultaneously coupled into two adjacent waveguides at the center of the array.

When the photons are coupled to two neighboring sites, $|\psi_0\rangle = a_0^\dagger a_1^\dagger |0\rangle$, the correlation map is given by

$$\Gamma_{p,q} = |E_{p,0}E_{q,1} + E_{p,1}E_{q,0}|^2 \tag{2.26}$$

Now, the correlation map changed considerably as shown in Fig.2.6.

The vanishing of the off-diagonal lobes indicates that both photons tend to bunch into the same side of the array. In other words, two paths lead to a coincidence measurement between waveguide p and q: either the photon from waveguide 0 travels towards waveguide p and the photon from waveguide 1 travels to waveguide q, or

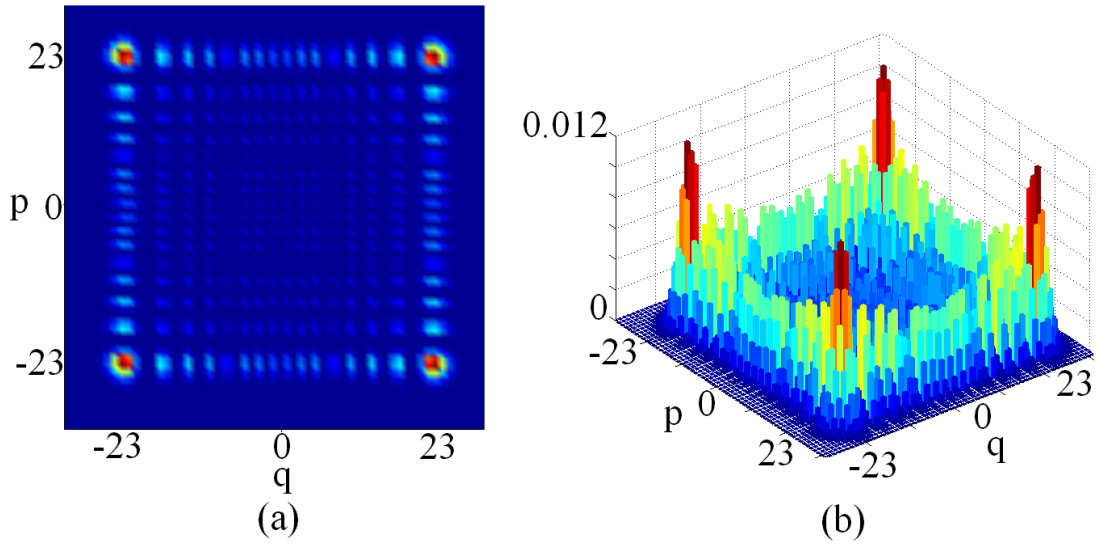

Figure 2.5: **(a) top view of the calculated correlation matrix $\Gamma_{p,q}$ representing the probability to detect at the output of the array exactly one photon at waveguide p and one photon at waveguide q, when both photons are coupled into the zeroth channel, and (b) side view of the correlation matrix.**

viceversa. In general, probability amplitude for a photon traveling from a particular waveguide at the input to another at the output are complex. Thus the interference between them lead to the disappearance of the off-diagonal lobes into the correlation matrix. Therefore, such an effect can be thought as a generalization of the Hong-Ou-Mandel experiment. The destructive interference which leads to vanishing of the off-diagonal lobes can be attributed to the inherent 90^o phase shift associated with nearest-neighbor coupling.

1-C) The two photons are simultaneously coupled into two waveguides

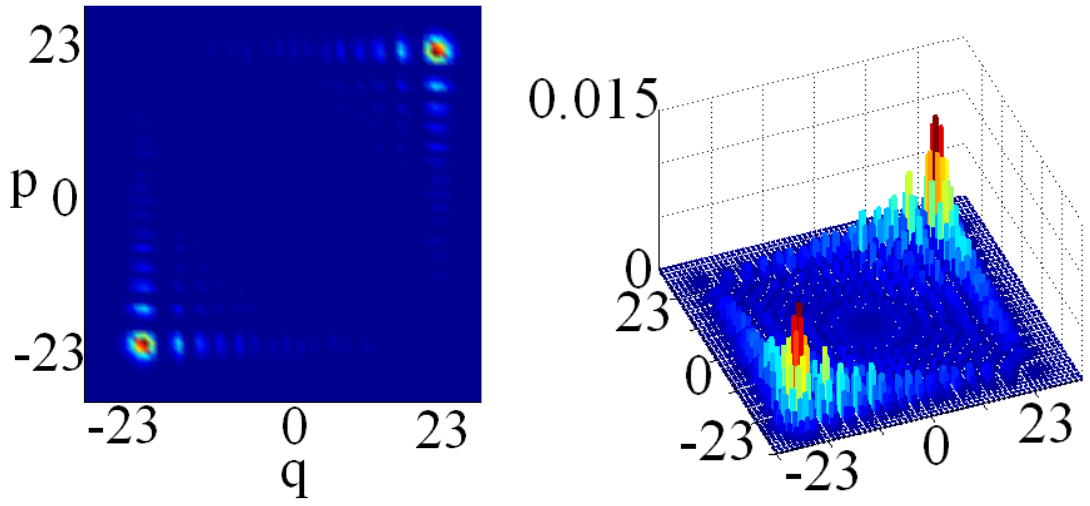

Figure 2.6: **(Left) Top view of the calculated correlation matrix, $\Gamma_{p,q}$, at $Z =$ 12 when the photons are coupled into the first and the second channels. This correlation map reveals that the highest probability of a coincidence measurement occurs either at waveguide 23 or at waveguide -23. (Left) Side view of the correlation matrix.**

separated by one waveguide.

In this case, the input state $|\psi_0\rangle = a^\dagger_{-1} a^\dagger_1 |0\rangle$, yields to the correlation

$$\Gamma_{p,q} = |E_{p,-1}E_{q,1} + E_{p,1}E_{q,-1}|^2. \tag{2.27}$$

Note that Eqn.(2.27) has the same form as Eqn.(2.26), but now the correlation map exhibits once again four lobes as shown in fig.2.7.

The photon pair exhibits bunching but with a different symmetry: if one photon is detected in between the lobes , the probability to detect its twin in a lobe vanishes,

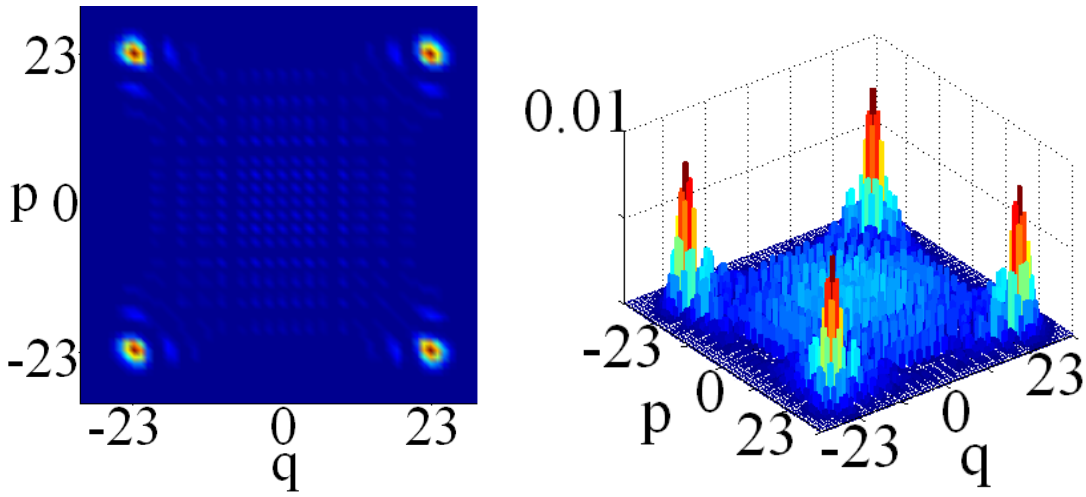

Figure 2.7: **(Left) Top , and (Right) side view of the correlation map.**

even though a single photon is most likely to reach the lobes. On the other hand, if one photon is detected in a lobe, it is also highly probable to find the second photon either in the same side of the array or in the opposite side.

2.2.2 Case 2: Path-entangled pair of photons as input

2-A) Path-entangled pair of photons in adjacent waveguides.

Consider the input state with two photons coupled in either of two neighboring waveguides

$$|\psi_0\rangle = \frac{1}{2}\left[\left(a_0^\dagger\right)^2 + \exp\left(i\phi\right)\left(a_1^\dagger\right)^2\right]|0\rangle$$

If we consider $\phi = 0$, the corresponding correlation map, $\Gamma_{p,q} = |E_{p,0}E_{q,0} + E_{p,1}E_{q,1}|^2$, is again a superposition of probability amplitudes. It is presented in

Fig.2.8, and shows that the diagonal peaks completely vanishes and it is significant only in the off-diagonal peaks.

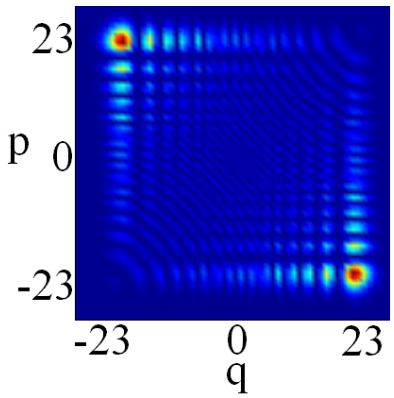

Figure 2.8: **Correlation map obtained from a path-entangled pair of photons injected into adjacent waveguides.**

Accordingly, both photons will always separate and emerge from different sides of the lattice. This photon antibunching processes emerge as consequence of the destructive interference between the complex probability amplitude.

Now, by introducing a phase shifting of $\phi = \pi$ between the two corresponding input ports, the correlation matrix becomes: $\Gamma_{p,q} = |E_{p,0}E_{q,0} - E_{p,1}E_{q,1}|^2$. Under such conditions, the photons emerge in either of two next-nearest-neighboring waveguides, yet with a π-phase shift as it is shown in Fig.2.9. In this case one photon will always reach a lobe while the other will always reach the center.

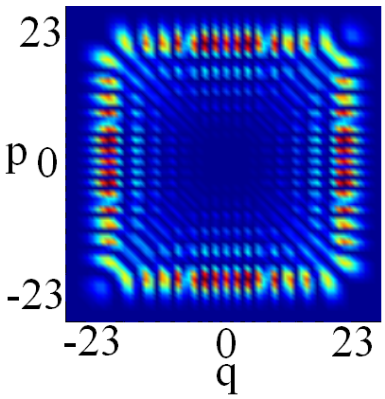

Figure 2.9: **Correlation map obtained from a path-entangled pair of photons injected into adjacent waveguides.**

2.2.3 Case 3: Pair of photons in the quantum lithography scheme.

3-A) Entangled pair of photons with correlated position.

So far we have considered single photon states as inputs, now we turn to the case when the photons are correlated in position, i.e., the input states states are given by

$$|\psi_0\rangle = \frac{1}{\sqrt{N}}(|2\rangle_l |0\rangle_{l+1} |0\rangle_{l+2} ... |0\rangle_h + |0\rangle_l |2\rangle_{l+1} |0\rangle_{l+2} ... |0\rangle_h +$$

$$|0\rangle_l |0\rangle_{l+1} |2\rangle_{l+2} ... |0\rangle_h + ... + |0\rangle_l |0\rangle_{l+1} |0\rangle_{l+2} ... |2\rangle_h).$$

This state describes the physical situation when the photon pair is always coupled to the same waveguide from a window of $N = h - l$ channels, but we have no

knowledge about which waveguide that was. The degree of entanglement of such a state depends on the width of the window size, N, larger window corresponds to stronger entanglement. The output coincidence rate is

$$\Gamma_{p,q} = \langle a_p^\dagger a_q^\dagger a_q a_p \rangle = \left| \sum_{k=l}^{h} E_{p,k} E_{q,k} \right|^2 . \tag{2.28}$$

In order to understand the consequences of Eq.(2.28), we consider an excitation window of 10 channels in a waveguide array of 100 elements. Thus, for this particular case the input state is written as follows

$$|\psi_0\rangle = \frac{1}{\sqrt{10}}(|0\rangle_1 ... |0\rangle_{44} |2\rangle_{45} |0\rangle_{46} ... |0\rangle_{100} + |0\rangle_1 ... |0\rangle_{45} |2\rangle_{46} |0\rangle_{47} ... |0\rangle_{100} + ...$$

$$|0\rangle_1 ... |0\rangle_{53} |2\rangle_{54} |0\rangle_{55} ... |0\rangle_{100} + |0\rangle_1 ... |0\rangle_{54} |2\rangle_{55} |0\rangle_{56} ... |0\rangle_{100}).$$

where the subscripts represent the number of waveguide. In Fig.2.10 we show the evolution of $\Gamma_{p,q}$ for various values of Z.

Surprisingly, along the diagonal, $p = q$, these correlation matrices exhibit the same probability distribution as that impulse response resulting from the same array having twice the physical length. Figs(.2.10- d, e, f) depict the probability distributions along the diagonal $p = q$, and they also correspond with the probability distributions obtained by exciting the central channel of the same array at $Z = 2, 6, 12$, respectively.

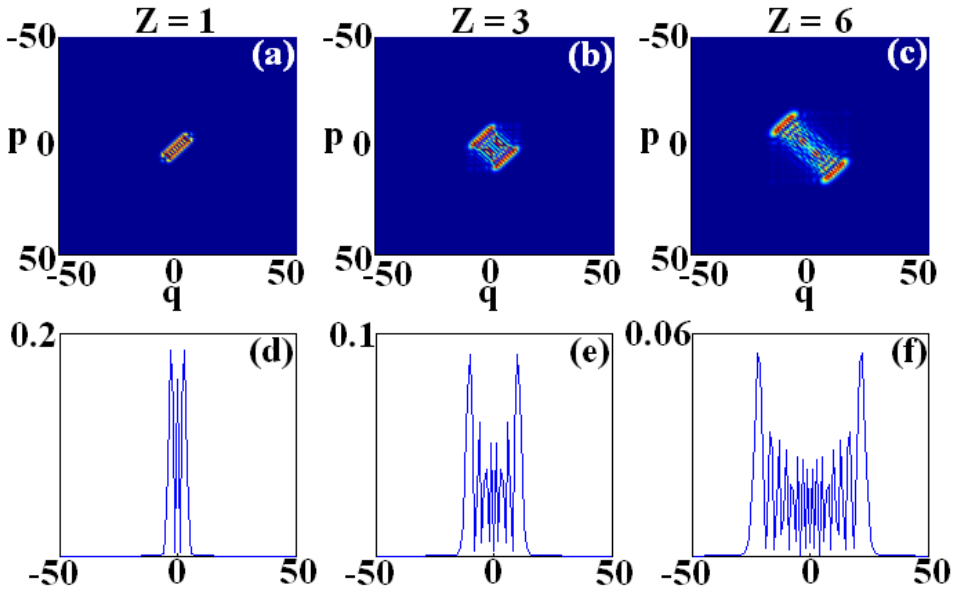

Figure 2.10: **(a, b, c) Output coincidence rate for various propagation distances. (d, e, f) Probability distributions along the diagonal $p = q$.**

It is also important to examine how the width of the excitation window affect the evolution of the correlation matrix. To do so we consider four different window sizes, namely, $N = 30$, 14, 2, and 1.

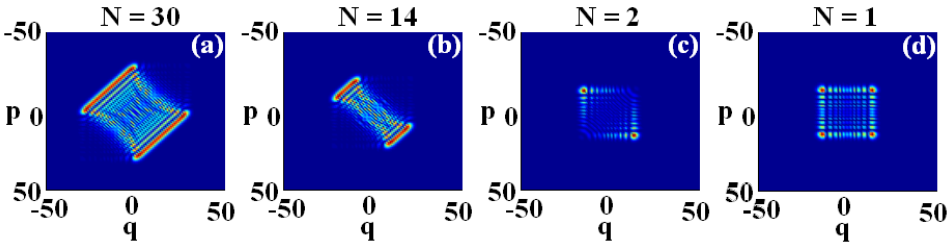

Figure 2.11: **(a, b, c) Effect of entangled-photon source size.**

As N decreases the strength of the two photon correlations decreases, and the

two photons become uncorrelated when the source is reduced to a point. In Figs.2.11 we depict $\Gamma_{p,q}$ for a periodic array while decreasing N from 30 to 1 in units of inter-waveguide separation. When $N = 1$, the two photons, no longer entangled, enter together one waveguide and $\Gamma_{p,q}$ factorizes into a product since the two photons are uncorrelated. As we increase N, the source becomes entangled and $\Gamma_{p,q}$ no longer factorizes. Note how the diagonal peaks (peaks along the line $p = -q$) are diminished and the two the two off-diagonal peaks are strengthened. Thus, $\Gamma_{p=-q,q}$ no longer corresponds to the classical output and the discrete diffraction features are washed out. On the other hand, $\Gamma_{p=q,q}$ approaches to the output intensity distribution for a point excitation at waveguide 50 with twice the length of the physical system as it was shown in Figs.(2.10).

3-B) Entangled pair of photons with anti-correlated position.

We now consider the entangled two-photon state when the two photons are anti-correlated in position:

$$|\psi_0\rangle = \frac{1}{\sqrt{r}}(|1\rangle_l ... |1\rangle_h + |0\rangle_l |1\rangle_{l+1} ... |1\rangle_{h-1} |0\rangle_h +$$

$$... + |0\rangle_l |0\rangle_{l+1} ... |1\rangle_{l+r} |1\rangle_{h-r} ... |0\rangle_{h-1} |0\rangle_h)$$

This case corresponds to the physical situation when the photons are always coupled to waveguides on opposite sides of a waveguide $r = (h - l)/2$ taken as

origin. For instance, in Fig2.12 where the pair of photons can be coupled into either waveguides $(r-3, r+3)$, $(r-2, r+2)$ or $(r-1, r+2)$.

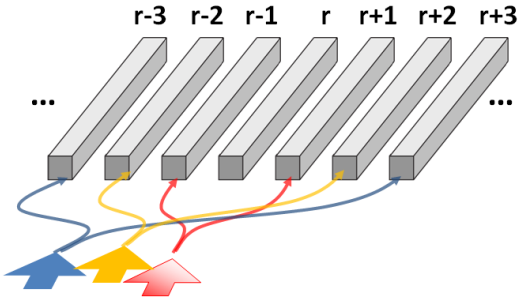

Figure 2.12: **Pair of photons separately coupled to a waveguide array on opposite sides of channel** r.

The output coincidence rate is then given by

$$\Gamma_{p,q} = \frac{1}{C}\left|\sum_{k=0}^{Q} E_{p,l+k}E_{q,h-k}\right|^2$$

where $Q = \frac{h+1}{2} - l$, $C = [(h-1)/2]^{-1}$. We find that the results are identical to the correlated case except that the diagonals $p = q$ and $p = -q$ are exchanged, as shown in figures 2.13 for a periodic waveguide array having 100 elements and several propagation distances.

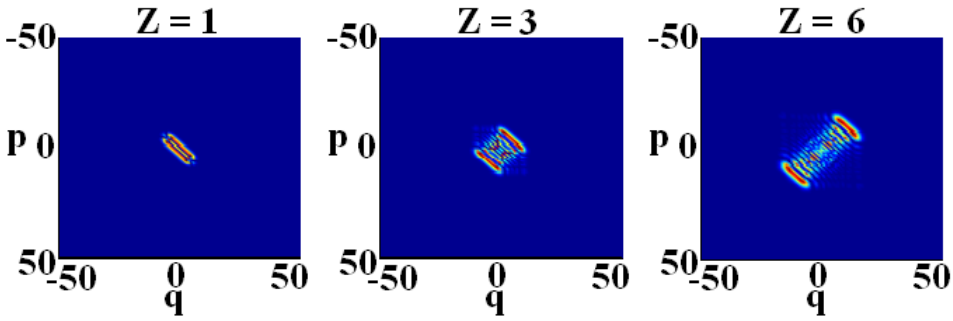

Figure 2.13: **Evolution of the correlation matrix for anti-correlated pair photons.**

Chapter 3

Glauber-Fock Photonic Lattices

3.1 Glauber-Fock Photonic Lattices

Since their introduction by Glauber in 1963, coherent states have been a subject of extensive research within the framework of quantum optics [30]. The average position and momentum of these minimum uncertainty wave-packets are known to follow the motion of a classical oscillator, thereby establishing an important bridge between classical and quantum mechanics. Coherent states arise as the eigenkets of the annihilation operator as well as from a displacement of the ground state of the quantized harmonic oscillator [27]. In general, if displacements of the oscillator eigenstates (termed Fock states or number states) are considered, a more general class of states, so called displaced Fock states (DFS), can be introduced [31, 32]. These states are of relevance to many areas of quantum optics, the most import-

ant one being the direct measurement of the Wigner quasi-probability distribution [33], which has been successfully performed on propagating coherent states [34] on single photons through cavities [35], and on motional states of trapped ions [36]. Furthermore, DFS constitute the eigenstates of Jaynes-Cummings systems with coherently driven atoms [37], and more recently, entangled DFS have been proposed for quantum dense coding [38]. DFS have been successfully generated by superposing s Fock state with a coherent state on a beam splitter [39]. However, due to the difficulties in generating pure Fock states of higher orders, this approach is limited to the lowest order DFS. To our knowledge, a direct observation of the genesis of these states has also not been possible to date.

The first section of this chapter is devoted to the theoretical study of a special semi-infinite photonic lattice of evanescently coupled waveguides, with a square-root distribution of the coupling between adjacent guides, which admits classical analogs to quantum coherent states and DFS [40]. Whereas, in section two we focus our attention to report a detailed description of the experimental observation of the classical analogues of coherent and displaced Fock states [41].

The general linear impulse response in these Glauber-Fock photonic lattices is described in closed form, and are markedly different from those occurring in other classes of optical arrays. The proposed lattices can be established by judiciously adjusting the separation distance between identical waveguide elements, in such a manner that the coupling constants vary as $\sqrt{n}$. The self-bending beam traject-

ories in such structures are analytically examined. A possible implementation of a Glauber-Fock array is shown in Fig. 3.1. In this system, the separation between successive identical single-mode waveguide elements is adjusted such that the inter-channel coupling varies as the square root of the site number n. This can be readily accomplished given that the coupling constant between waveguides depends exponentially with the separation distance d_n, $\kappa_{n,n+1} \sim \exp(-\gamma d_n)$ [44].

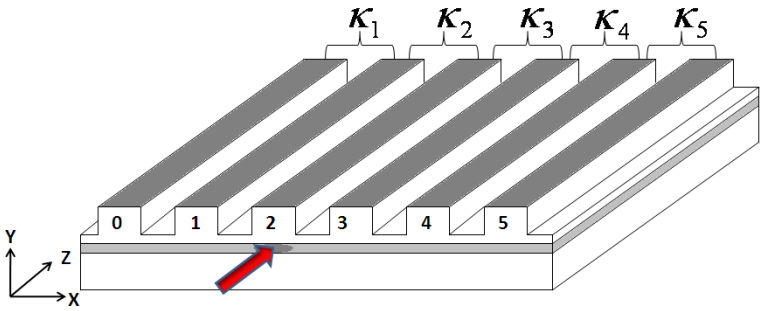

Figure 3.1: **Schematic view of a Glauber-Fock waveguide array.**

In the proposed system, the normalized modal field amplitudes obey a discrete linear Schrödinger-like equation:

$$\begin{aligned} i\frac{dE_0}{dZ} + E_1 = 0 \qquad (a) \\ i\frac{dE_n}{dZ} + \sqrt{n+1}E_{n+1} + \sqrt{n}E_{n-1} = 0 \qquad (b), \end{aligned} \tag{3.1}$$

where the first equation describes the field at the edge of the lattice ($n = 0$ waveguide site) and the second one stands for any other site ($n > 0$). The normalized coordinate Z is given by $Z = \kappa_1 z$, where z is the actual propagation distance and

κ_1 is the coupling coefficient between the site 0 and 1. We begin by exploring the stationary wave states allowed in this system. To do so, we assume the solution $E_n = a_n exp(i\mu Z)$ in Eq.(3.1), where μ is the propagation eigenvalue. The resulting linear difference equation takes the form

$$-\sqrt{n+1}a_{n+1} + \mu a_n - \sqrt{n}a_{n-1} = 0. \tag{3.2}$$

To solve Eq.(3.2) we make the substitution

$$a_n = \frac{f_n}{2^{n/2}}, \tag{3.3}$$

where f_n is a function of as yet unspecified argument x. On substituting Eq.(3.3) into Eq.(3.2), we obtain a recursion relation for f_n

$$\sqrt{n+1}f_{n+1} - \mu\sqrt{n}f_n + 2\sqrt{n}f_{n-1} = 0. \tag{3.4}$$

This is identical to the recursion relation

$$H_{n+1}(x) - 2xH_n(x) + 2nH_{n-1}(x) = 0, \tag{3.5}$$

for the Hermite polynomials H_n, provided that we choose $x = \mu/\sqrt{2}$ and $f_n = H_n/\sqrt{n!}$ [42]. Therefore, the stationary solution for these Galuber-Fock lattices becomes

$$a_n = \frac{H_n(\mu/\sqrt{2})}{2^{n/2}\sqrt{n!}}. \tag{3.6}$$

This expression (3.6) corresponds to the so-called supermodes of the lattice. Threfore, if were able to produce a physical semi-infinite Glauber-Fock lattice, by separately launching the supermodes through the array, they will remain invariant during propagation.

In order to obtain the impulse response of the Glauber-Fock lattice, i.e., when only one site is excited, we consider the following virtual x-representation:

$$i\frac{d\psi\left(x,Z\right)}{dZ}=-\left(a+a^{\dagger}\right)\psi\left(x,Z\right), \tag{3.7}$$

where the annihilation/creation operators are respectively defined as [**?**]

$$\begin{aligned} a&=\frac{1}{\sqrt{2}}\left(x+\frac{d}{dx}\right)\\ a^{\dagger}&=\frac{1}{\sqrt{2}}\left(x-\frac{d}{dx}\right), \end{aligned} \tag{3.8}$$

such that

$$a\psi_n(x)=\sqrt{n}\psi_{n-1}(x),$$

$$a\psi_n(x)=\sqrt{n+1}\psi_{n+1}(x),$$

where the system's eigenfunctions are given by the Gauss-Hermite functions

$$\psi_n(x)=\frac{1}{\sqrt{\pi^{1/2}2^n n!}}\exp\left(-x^2/2\right)H_n(x).$$

In order to simplify our notation we establish the correspondence $\psi_n(x)\rightarrow|n\rangle$. On the other hand, the set of eigenfunctions $|n\rangle$ is complete and orthonormal, thus

we can always represent an arbitrary square-integrable function, $\Psi(x, Z)$, by an expansion in a series of $|n\rangle$

$$\psi(x, Z) = \sum_{n=0}^{\infty} E_n(Z)\,|n\rangle\,. \tag{3.9}$$

Then, by sustituting Eq.(3.9) into Eq.(3.7) yields

$$i\sum_{n=0}^{\infty} \frac{dE_n(Z)}{dZ}\,|n\rangle = -\sum_{n=0}^{\infty}\left(\sqrt{n}E_n(Z)\,|n-1\rangle + \sqrt{n+1}E_n(Z)\,|n+1\rangle\right). \tag{3.10}$$

Using orthonormality properties of the eigenfunctions $|n\rangle$, we finally derive Eq.(3.1). Thus, by eliminating the virtual x-dependence in Eq.(3.7) we have effectively obtained the equations governing light evolution in the systems under investigation. Eq.(3.7) can be readily solved using the evolution operator

$$\psi(x, Z) = \exp\left(iZ\left[a + a^{\dagger}\right]\right)\psi(x, Z = 0)\,. \tag{3.11}$$

Note that $\hat{D}(iZ) = \exp\left(iZ\left[a + a^{\dagger}\right]\right)$ represents the so-called Glauber displacement operator in quantum optics []. Since the operators a, and $a^{\dagger}$ satisfy the commutation relation $[a, a^{\dagger}] = 1$, and $[a, [a, a^{\dagger}]] = [a^{\dagger}, [a, a^{\dagger}]] = 0$, we can factorize $\hat{D}(iZ)$ through the Baker-Hausdorff formula

$$\hat{D}(iZ) = \exp\left(-Z^2/2\right)\exp\left(iZa^{\dagger}\right)\exp(iZa)\,. \tag{3.12}$$

The initial condition $\psi(x, Z=0)$, i.e. the field at the input of the lattice, can be described in general via a linear superposition of *states*, depending on which waveguides are excited. The aim here is to analyze the case when light is launched into a single lattice site at position k from the edge (impulse response). So, the input field can be written as: $\psi(x, Z=0) = \sum_{n=0}^{\infty} E_n(Z=0)\,|n\rangle = |k\rangle$. Where we have considered a field amplitude $E_n(Z=0) = 1$. In this case, Eq.(3.11) becomes

$$\sum_{n=0}^{\infty} E_n(Z)\,|n\rangle = \exp\left(-Z^2/2\right)\exp\left(iZa^{\dagger}\right)\exp\left(iZa\right)|k\rangle\,. \tag{3.13}$$

To evaluate the field distribution in the *m-th* waveguide we must take the inner product $\langle m|\sum_{n=0}^{\infty} E_n(Z)\,|n\rangle$, hence

$$E_m(Z) = \exp\left(-Z^2/2\right)\langle m|\exp\left(iZa^{\dagger}\right)\exp\left(iZa\right)|k\rangle\,. \tag{3.14}$$

To develop an analytical expression for the solution of Eqs.(3.1), a Taylor series expansion for the exponentials of the a, and $a^{\dagger}$ operators in Eq.(3.14) is performed (see appendix **??**). For $m = k + s$ (where s=0, 1, 2, ...), i.e., for sites $m \geqslant k$(on the right of the excited waveguide k), the field at a distance Z is given by

$$E_{k+s}(Z) = \exp(-Z^2/2)(iZ)^s\sqrt{\frac{k!}{(k+s)!}}L_k^s(Z^2), \tag{3.15}$$

where $L_k^s(Z^2)$ represents the generalized Laguerre polynomials of degree k []. Conversely, if $m = k - s$, the field at any position to the left side of the excited

waveguide, is

$$E_{k-s}(Z) = \exp(-Z^2/2)(iZ)^s \sqrt{\frac{(k-s)!}{k!}} L_{k-s}^s(Z^2). \tag{3.16}$$

When $k = 0$, i.e., when light is injected into the first waveguide, Eq.(3.15) readily reduces to the field distribution

$$E_m(Z) = \exp(-Z^2/2)(iZ)^m/\sqrt{m!}. \tag{3.17}$$

Figure 3.2. depicts the intensity evolution among waveguide sites in this Glauber-Fock lattice when the first element is initially excited.

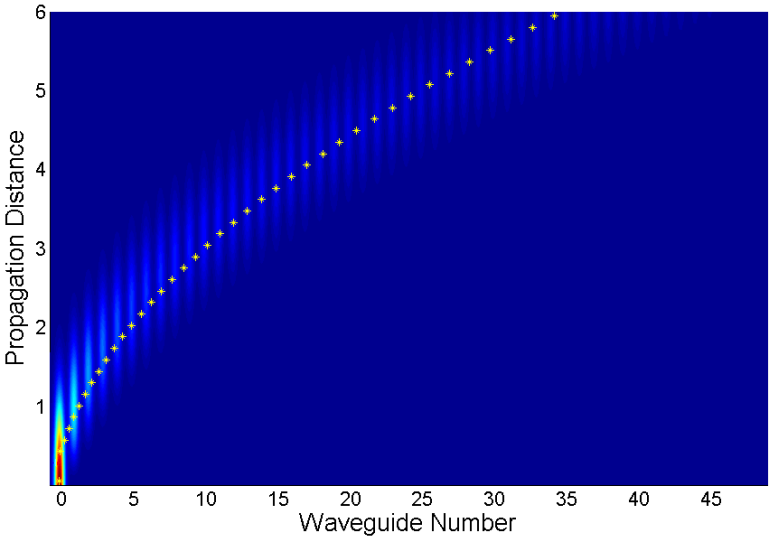

Figure 3.2: **Intensity light evolution through a Glauber-Fock waveguide array having 45 elements.**

Notably, the expression for $E_m(Z)$ in Eq.(3.16) is identical in form with the com-

plex amplitudes involved between Fock and coherent states in quantum optics [27]. The resulting intensity distribution $I_m = |E_m|$ at any distance $Z \neq 0$ is Poissoanian with m resembling the probability of finding a quantum harmonic oscillator at an energy level m, if a measurement is made when the oscillator is in a coherent state. In other words, for the particular case $|k\rangle = |0\rangle$, we can think of the entire propagating lattice field as the classical analog of a quantum coherent state evaluated on the imaginary axis "iZ"

$$|\alpha = iZ\rangle = \exp(-|\alpha|^2/2) \sum_{n=0}^{\infty} \frac{(\alpha)^n}{\sqrt{n!}} |n\rangle \,, \tag{3.18}$$

whereas the vacuum state itself corresponds to the incoming field into the $0-th$ waveguide. The role of the displacement operator, the generator of the coherent states, is played by the lattice itself on the field. As light propagates along the array, the energy spreads from the left to the right (Fig.3.2) . And the trajectory where the intensity is a maximum can be accurately described by the function

$$Z = f(n) = \exp\left(\frac{1}{2}\left[-\gamma + \sum_{k=1}^{n} \frac{1}{|k|}\right]\right), \tag{3.19}$$

where γ is the Euler-Mascheroni constant ($\gamma = 0.57721$). Direct numerical simulations (dashed line in Fig.3.2) are in excellent agreement with Eq.(3.19).

Along similar lines, a classical number state $|k\rangle$ correspond to the initial excitation of the $k-th$ waveguide site. In this case, the field distribution given by

Eqs.(3.15), and (3.16) represent the matrix elements of the Glauber displacement operator $\langle m| D(iZ) |k\rangle$ in a Fock base representation. Figs. (3.3), (3.4), and (3.5) illustrate, and compares the intensity evolution in the same structure when four different sites are excited. Note that there is a marked difference between discrete diffraction occurring in regular waveguide arrays with that expected in a semi-infinite Glauber-Fock lattice. In the latter structures the intensity patterns are always tilted and guided towards the high coupling region, a direct outcome of the imposed $\sqrt{n}$ coupling law. The characteristic $(k+1)$-humped intensity profile of the displaced number states resulting from the boundary reflection is evident in the numerical simulations.

3.2 Observation of Galuber-Fock dynamics in photonic lattices.

As we showed in the last section, a photonic lattice of evanescently coupled waveguides [40], obeying a square-root law distribution for the coupling between adjacent guides, allows us for a direct observation of a classical analogue for the displacement of Fock states. In these Glauber-Fock photonic lattices, every excited waveguide is associated with a Fock state and the spatial evolution of the light field corresponds to the probability amplitudes of the displaced Fock states (DFS) in the number basis. Thereby, the emergence of these fundamental states and the underlying dis-

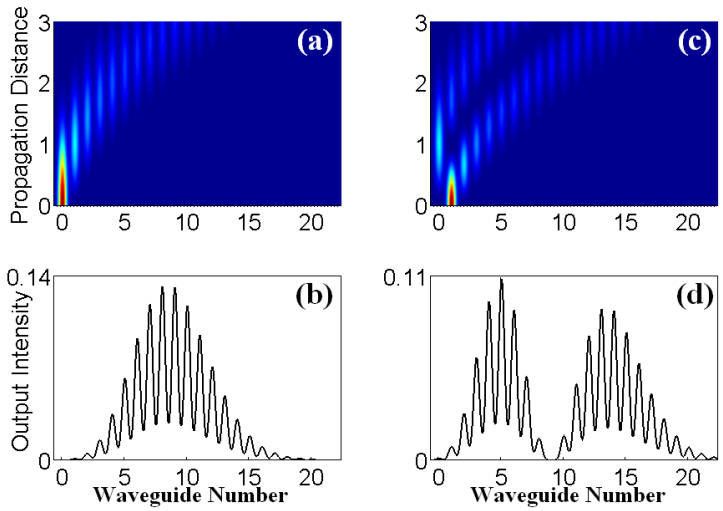

Figure 3.3: **(a) Intensity evolution of a classical coherent state, and (b) its corresponding output intensity distribution at Z=3. Similarly, for the (c) first classical displaced Fock state, and (d) its corresponding intensity profile at Z=3**

placement process can be visualized. As no collapse of the wavefunction occurs for classical light, the displacement can be observed for a wide range of displacement amplitudes simultaneously.

In this section, we present the first experimental realization of a Glauber-Fock photonic lattice and directly observe the classical analogue of Fock state displacements up to the fourth oscillator eigenstate. This arrangement is implemented by direct femtosecond (fs) laser waveguide inscription in fused silica [44], whereby the required coupling distribution is achieved by a controlled variation of the distance

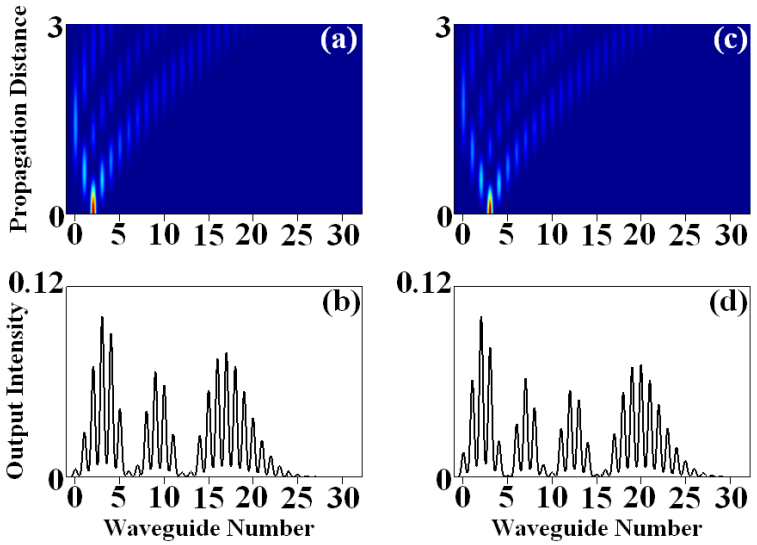

Figure 3.4: **(a, c) Intensity evolution of a classical second, and third displaced Fock state, and (b, d) their corresponding output intensity distribution at Z=3.**

between neighboring waveguides.

As we wrote before, in order to observe the displacement of Fock states in the optical domain, one requires a lattice of single-mode waveguides, whose coupling coefficients between adjacent elements vary with the square-root of the site labelling index n:

$$i\frac{dE_n}{dZ} + C_{n+1}E_{n+1} + C_nE_{n-1} = 0; \qquad C_n = \sqrt{n}C_1. \tag{3.20}$$

Thereby, E_n denotes the modal amplitude in guide n, Z is the longitudinal coordinate and C_1 is the coupling strength between the first two waveguides (see

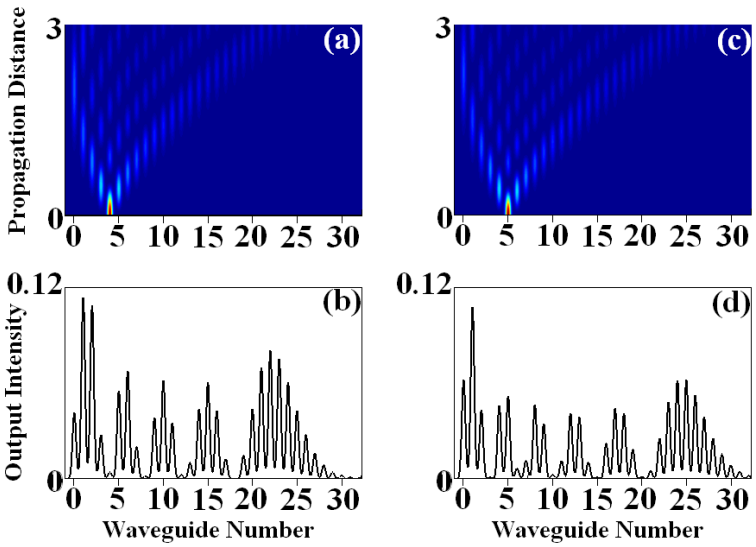

Figure 3.5: **(a, c) Intensity evolution of a classical fourth and fifth displaced Fock state, and (b, d) their corresponding output intensity distribution at Z=3.**

Fig.3.7).

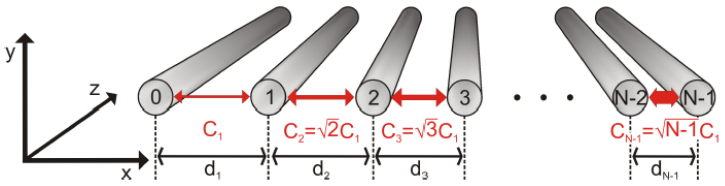

Figure 3.6: **Schematic view of a Glauber-Fock waveguide lattice of N waveguides with a square root increase of the coupling strength $C_n \propto \sqrt{n}$.**

In the weak coupling regime C_n is governed by the overlap of the waveguide modes with the electric permittivity profile [44]. In this case, the coupling depends

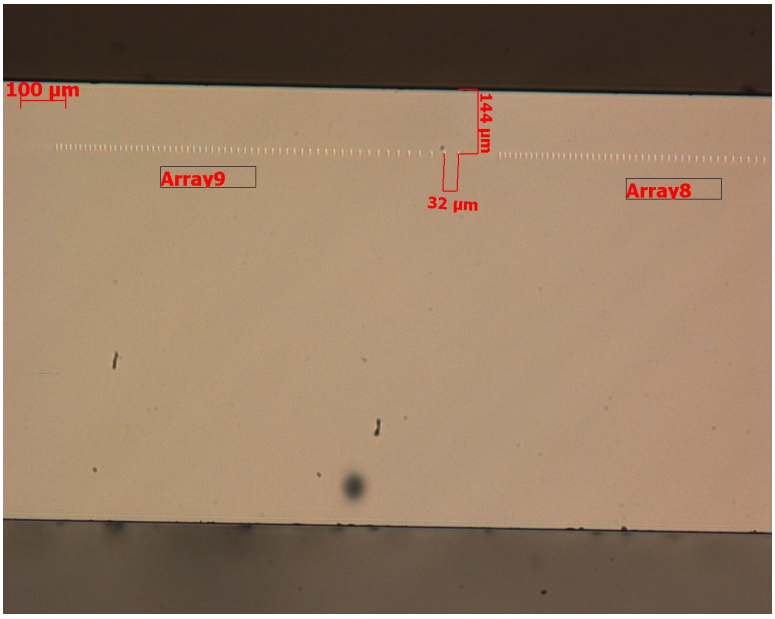

Figure 3.7: **Top view of the actual Glauber-Fock arrays inscribed in fused silica.**

exponentially on the distance between the guides: $C_n = C_1 \exp\left(-\left[d_n - d_1\right]/\kappa\right)$, with κ and d_1 being exponential fit parameters, if C_1 is predetermined. This dependence has been experimentally verified for fs laser-written waveguides over a wide range of separations [44]. Consequently, the coupling dependence of Eq. (3.20) is readily achieved by inscribing the waveguides with $d_n = d_1 - \kappa \lg \sqrt{n}$ as the distribution of separations.

In our setting the oscillator eigenstates are represented by single waveguides, i.e., the Fock state $|k\rangle$ shall correspond to the situation when only guide k is excited: $E_n = \delta_{n,k}$. If light is launched into this single site at $z = 0$, the light propagation

along z will map the displacement of the Fock state $|k\rangle$ along the imaginary axis of the quadrature phase space. More specifically, the field amplitudes evolve analogous to the matrix elements of the unitary displacement operator $D(\alpha) = \exp\left(\alpha a^{\dagger} - \alpha^{*} a\right)$ [30]:

$$E_n(Z) = \langle n| D(iC_1 Z) |k\rangle \tag{3.21}$$

with $a^{(\dagger)}$ being the ladder operators of the oscillator: $a^{\dagger} |n\rangle = \sqrt{n+1}\,|n+1\rangle$, $a\,|n\rangle = \sqrt{n}\,|n-1\rangle$. Hence, after propagating a distance Z, the light intensity distribution, $|E_n|^2 = |\langle n| D(iZC_1) |k\rangle|^2$, is equivalent to the number distribution of the DFS: $D(iZC_1)\,|k\rangle$ [31].

In our experiments, we measured the dependence of coupling on waveguide separation at a wavelength of $\lambda = 633nm$ and found the parameters $d1 = 23\mu m$ and $\kappa = 5.5\mu m$ for a desired coupling of $C_1 = 0.371cm^{-1}$. Using these results, we inscribed a Glauber-Fock lattice with N = 59 waveguides and $10cm$ length in fused silica, corresponding to a maximum displacement amplitude $\lambda = 3.7i$. We employed fluorescence microscopy to directly observe the intensity evolution of the injected light [45] and imaged the output intensity patterns onto a CCD camera.

Figs. 4.2(a-d) present numerical results obtained from integrating Eq.(3.20) for several different input sites while the experimental data is shown in Figs.4.2(e-h), matching the theoretical expectations very closely. The results clearly map the genesis of coherent states with their typical Poisson distribution from the displace-

ment of the ground state of the oscillator Figs.4.2(a, e) as well as the generation of higher-order DFS from its higher eigenstates Figs.4.2 (b-d, f-h).

Note, that the right-hand boundary at $n = N-1$ is not reached by the propagating light. Thus, the lattice can be considered as effectively semi-infinite, corresponding to the semi-infinite set of Fock states. The largest coupling reported for laser written waveguide arrays is $C_{N-1} \propto 5.5cm^{-1}$ [46], which limits the maximum number of waveguides for the given C_1 to $N \propto 200$. As these measurements demonstrate, Glauber-Fock lattices support an optical emulation of DFS for a wide range of parameters, providing direct insight into their generation characteristics. The success of such an optical emulation clearly highlights the wave nature of DFS. As governed by Eq.(3.21), the phases of the Fock coefficients are also encoded in the modal amplitudes. Hence, a full reconstruction of the DFS could be achieved by interferometric phase retrieval at the end of the lattice, e.g., by superposing the output field with a reference wave and phase-stepping [47].

In conclusion, we established the theory directly observed a classical analogue for the displacement of Fock states by monitoring the propagation of classical light waves in Glauber-Fock photonic lattices.

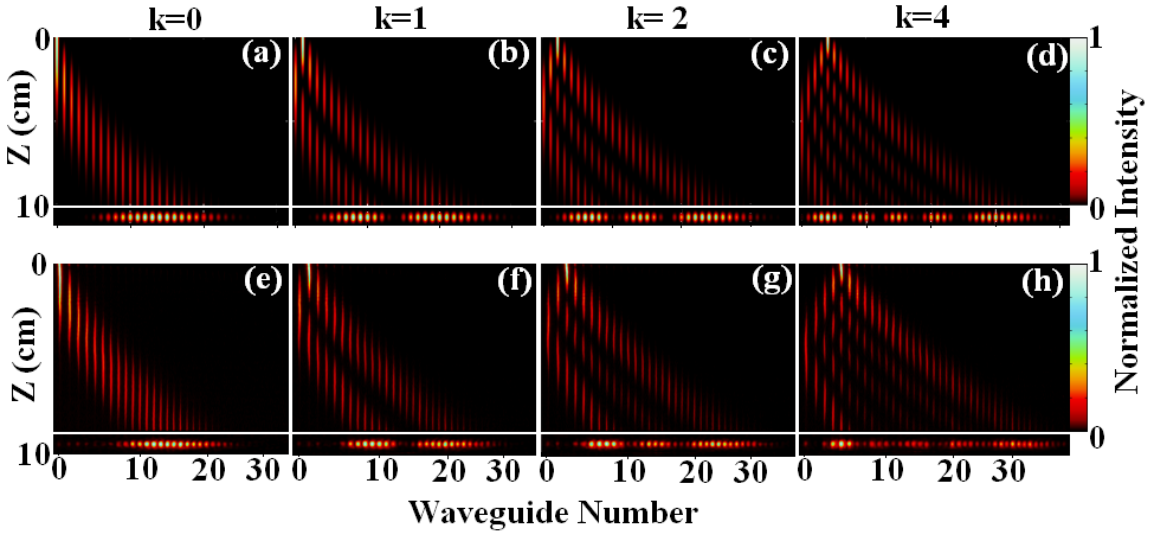

Figure 3.8: **Light propagation in a** $10cm$ **long Glauber-Fock lattice of 59 waveguides, acting as an optical analogue of Fock state displacement. (a-d) Calculated intensity evolution and output intensity profiles for** $C_1 = 0.37cm^{-1}$ **and the input (a)** $k = 0$**, (b)** $k = 1$**, (c)** $k = 2$**, and (d)** $k = 4$ **sites representing the displacement of the Fock states (a)** $|0\rangle$**, (b)** $|1\rangle$**, (c)** $|2\rangle$**, and (d)** $|4\rangle$**, respectively. (e-h) Experimental fluorescent images of the intensity evolution and nearfield images of the output facet for a single-waveguide excitation of these sites with** $\lambda = 633nm$**. All images have been normalized to their respective peak intensity. For generality, the theoretical images are shown for equidistant waveguides, while in the experiments the sites are distributed according to** $d_n = d_1 - \kappa \log(\sqrt{n})$**.**

Chapter 4

Quantum Correlations in Glauber-Fock photonic lattices.

4.1 Quantum Correlations in Glauber-Fock photonic lattices

As we shall show in this chapter, Glauber-Fock lattices provide a fertile ground for quantum random walks (QRWs) of correlated particles. In chapter 2 we studied the evolution quantum states through uniform waveguide lattices. We found that quantum interference of all possible paths lead to the correlation of the photons [28], thereby enabling us to study in continuous time QRWs in the correlation space [48]. Correlation of identical particles has been analyzed for disordered lattices ex-

hibiting Anderson localization [49] and for Bloch oscillations occurring in lattices with a linear gradient in their propagation constant [50]. In the aforementioned cases, however, those lattices are shift-invariant and infinite in the transverse dimension. Hence, possible trajectories in a QRW are independent of their starting point. Breaking this invariance and introducing a boundary can thus embed the additional degree of freedom of transverse position into the QRW. We therefore analyze the correlations for pairs of separable and path-entangled photons as well as of (notional) fermions in a semi-infinite Glauber-Fock lattice and show how their correlation patterns uniquely depend on the input position.

As evident from the experimental observations and from the numerical solutions, Fig. 4.2, a classical light field launched into site k exhibits an output intensity distribution with $k + 1$ maxima, and is therefore highly characteristic for its input waveguide. Hence, the same feature applies to the output probability distribution of a single photon. When a single photon is injected into the first waveguide (i.e., the 0-*th* channel), the photon spreads across the lattice by coupling from one waveguide to its neighbors in different patterns depending on which waveguide is the photon injected. Figs. 4.2(a-c) show the expected distribution for a single photon excitation of the first three sites. On the other hand, if two indistinguishable photons propagate in the lattice, all possible paths will interfere, and one can therefore expect correlation patterns which are unique for each combination of input positions, in contrast to the correlations arising in uniform lattices (see chapter 2) where all

waveguides are embedded in identical coupling environments.

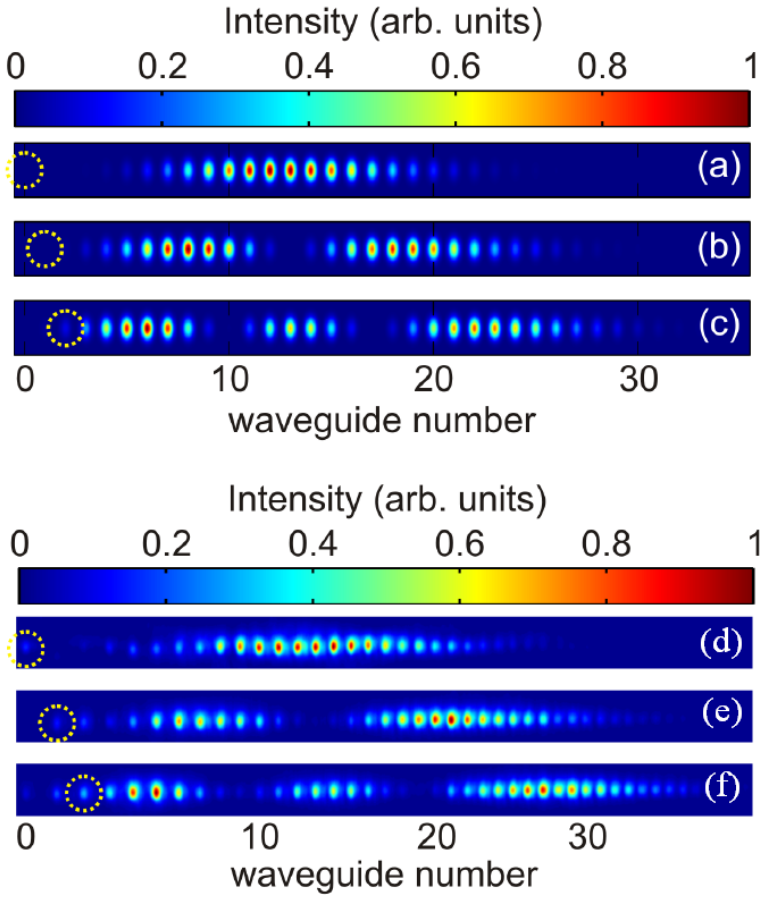

Figure 4.1: **The sample length was 10cm and $C_1 = 0.36cm^{-1}$. (a-c) Numerically calculated output intensities for the input sites (a) k = 0, (b) k = 1 and (c) k = 2. (d-f) Experimentally measured classical output intensities at $\lambda = 800nm$. All images have been normalized to their respective peak values.**

At first, we consider input states of separable photons, where one photon is launched into each of the two waveguides k and l: $a_k^\dagger a_l^\dagger |0\rangle$. The probability of

coincident detection of photons in guides q and r is determined by the photon number correlation

$$\Gamma_{q,r} = \left\langle a_q^\dagger a_r^\dagger a_r a_q \right\rangle = \left| E_{q,k} E_{r,l} + E_{q,l} E_{r,k} \right|^2 , \tag{4.1}$$

where

$$\begin{aligned} E_{m,n}(Z) &= \exp\left(-Z^2/2\right) (iZ)^{n-m} \sqrt{\frac{m!}{n!}} L_m^{n-m}\left(Z^2\right), \qquad for \qquad m < n \\ E_{m,n}(Z) &= \exp\left(-Z^2/2\right) (iZ)^{m-n} \sqrt{\frac{n!}{m!}} L_m^{m-n}\left(Z^2\right), \qquad for \qquad m > n \end{aligned} \tag{4.2}$$

and L_s^k are the generalized Laguerre polynomials of degree k. We calculated $\Gamma_{q,r}$ for a $10cm$ long semi-infinite lattice with $C_1 = 0.36cm^{-1}$ for a set of input configurations involving the first three sites [Figs. 4.2(a-g)]. The correlation patterns, and thereby the trajectories of a correlated QRW, are unique for each input state and, notably, resemble the transverse field modes of light in a resonator. Even for a constant separation of the input waveguides, Γ depends strongly on the distance to the boundary of the lattice, Figs.4.2, clearly revealing the broken shift invariance. The correlations further show typical bosonic bunching behavior: on-diagonal peaks, corresponding to a high probability of detecting both photons in the same output region.

Next we consider the propagation of a path-entangled input state with two photons in either of two waveguides: $|\psi\rangle = \frac{1}{2}\left(a_k^{\dagger 2} \pm a_l^{\dagger 2}\right)|0\rangle$. These biphoton states are the lowest order N00N-states, a class of maximally entangled N-photon states

[51]. Upon propagation of such a state in a photonic lattice the photon correlation yields

$$\Gamma_{q,r} = |E_{q,k}E_{r,k} \pm E_{q,l}E_{r,l}|^2 \tag{4.3}$$

The correlations have been calculated for the symmetric (+) as well as for the antisymmetric state (-) [Figs. 4.3, 4.4]. As before, the correlation maps are highly distinct for each particular input configuration. Figs. 4.3 correspond to the correlation map for path entangled input states coupled into adjacent waveguides clse to the left boundary, whereas Figs.4.4 stand for states separated by one channel.

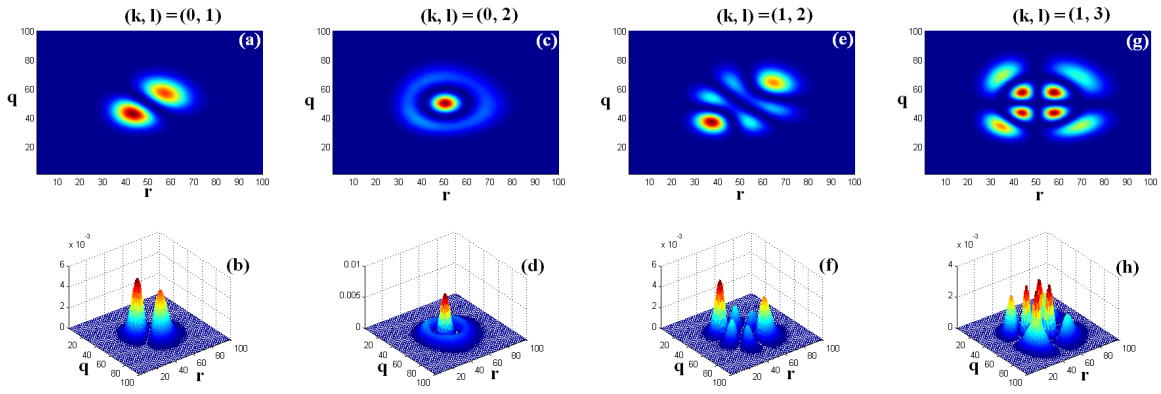

Figure 4.2: **Photon correlations in a Glauber-Fock array for the lattice parameters: sample length** $10cm$ **and** $C_1 = 0.36cm^{-1}$**. Calculated photon correlation for the input state** $|\psi\rangle = a_k^\dagger a_l^\dagger |0\rangle$ **with a) (k,l)=(0,1), c) (k,l)=(0,2), e) (k,l)=(1,2), and g) (k,l)=(1,3). (b, d, f, h) Side views corresponding to figures (a, c, e, g).**

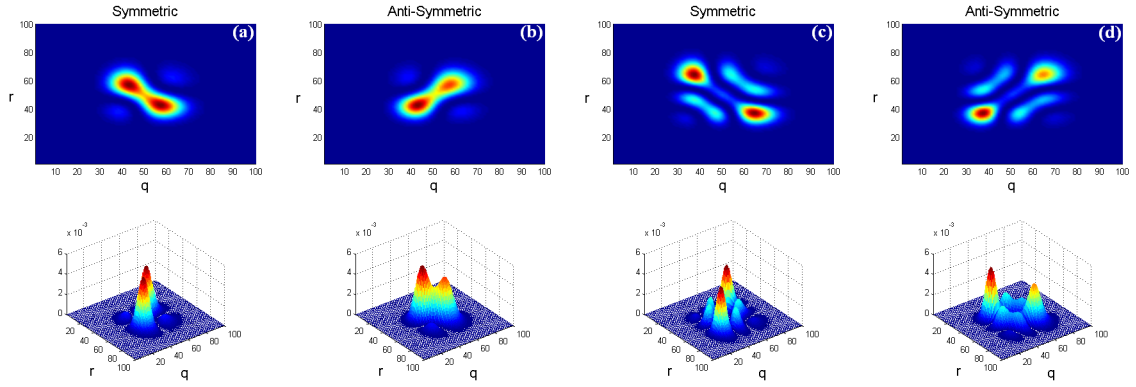

Figure 4.3: **Calculated photon correlation for the input state** $|\psi\rangle = \frac{1}{2}\left(a_k^{\dagger 2} \pm a_l^{\dagger 2}\right)|0\rangle$ **with (a, b) (k,l)=(0,1), and (c, d) (k,l)=(1,2). (Bottom) Side views.**

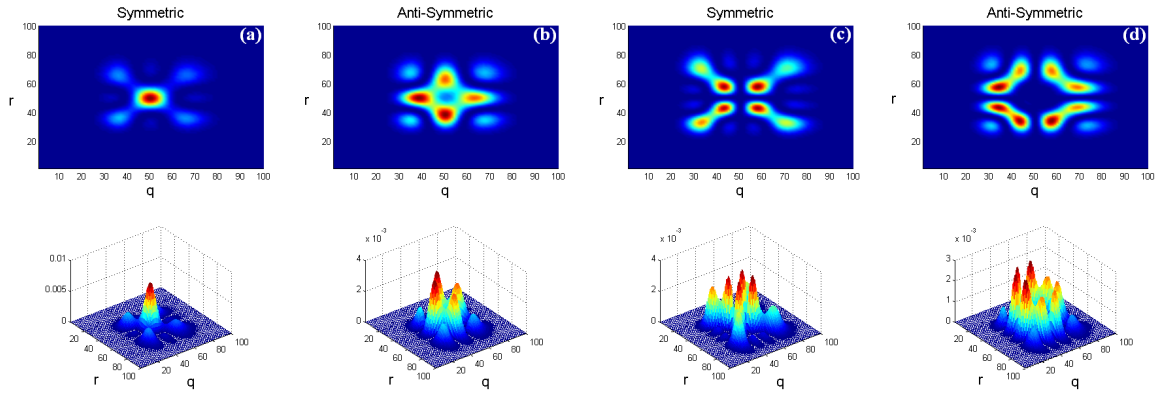

Figure 4.4: **Calculated photon correlation for the input state** $|\psi\rangle = \frac{1}{2}\left(a_k^{\dagger 2} \pm a_l^{\dagger 2}\right)|0\rangle$ **with (a, b) (k,l)=(0,2),and (c, d) (k,l)=(1,3). (Bottom) Side views.**

To gain a more thorough insight into the nature of these correlations, it is worthwile to compare them to the correlation of product states of identical bo-

sons [Eq.(4.1)] and fermions in Glauber-Fock lattices. While it is impossible to observe the correlations of fermions in waveguide lattices, they may well arise in other discrete systems, such as trapped atoms in optical lattices [52]. Introducing the annihilation(creation) operators $b_n^\dagger$ for fermions in a lattice and considering initial states of the type $|\psi^f\rangle = b_k^\dagger b_l^\dagger |0\rangle$, the fermionic correlation function yields to:

$$\Gamma_{q,r} = \left\langle b_q^\dagger b_r^\dagger b_r b_q \right\rangle = \left| E_{q,k} E_{r,l} - E_{q,l} E_{r,k} \right|^2 . \tag{4.4}$$

The results displayed in Figs. 4.5 second column show a strong anticorrelation: Off-diagonal peaks dominate the correlation map and there is zero probability to find both particles in the same channel. Quite remarkably, the correlation patterns for the entangled photons [Figs. 4.5 (third and fourth columns)] reveal a composition of bosonic bunching and fermionic antibunching features, similar to the situation in disordered lattices [49]. In some cases the main peaks follow a bosonic behavior, while in others the fermionic anticorrelation prevails. However, as the entangled photons are still bosons, they never exhibit the strong on-diagonal trench characteristic for fermions.

In conclusion, as every waveguide is subjected to a different coupling environment, correlations of identical particles evolving in such a lattice are highly characteristic for each input configuration. Therefore, quantum random walks exploiting the additional layer of complexity associated with this degree of freedom seem in reach.

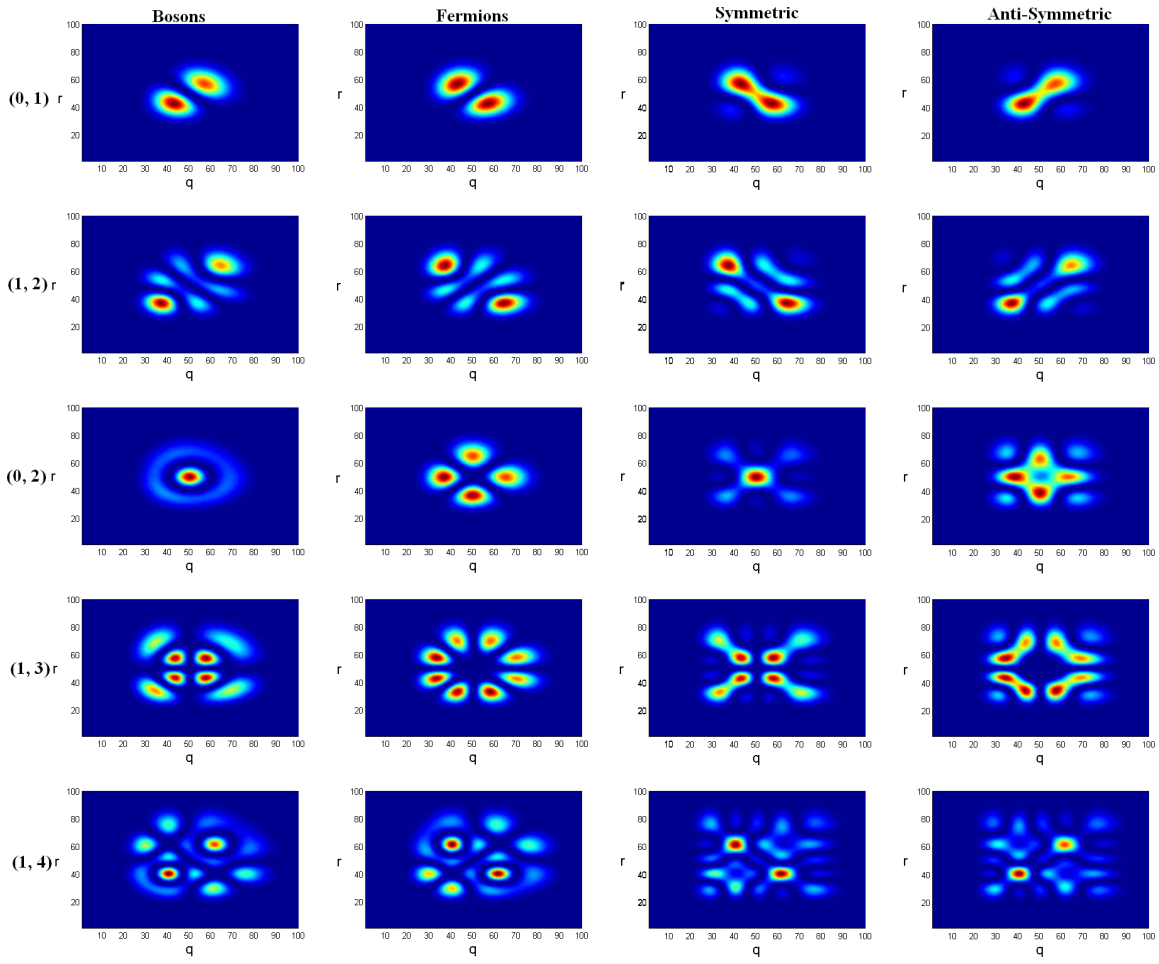

Figure 4.5: **Expected correlation patterns of single photons, separable fermions and path-entangled photons. The numbers on the left indicate the site position where the photons were launched. Second column shows the correlation function of two fermions being launched into the lattice.**

Chapter 5

Bloch-like dynamics in Glauber-Fock photonic lattices

5.1 Bloch-like dynamics in modulated-tilted Glauber-Fock photonic lattices

We demonstrate that single-photon revivals are possible in a new class of dynamic optical systems-the so-called Glauber-Fock oscillator lattices. In these arrays, both Bloch-like oscillations and dynamic delocalization can occur which can be described in closed form. More importantly, the bunching and anti-bunching response of path-entangled photons can be pre-engineered in such coupled optical arrangements. We elucidate these effects via pertinent examples and we discuss the prospect of

experimentally observing these quantum interactions.

Manipulation and engineering of quantum states has become an issue of great importance within the framework of quantum information and computation. Along these lines, several physical platforms have been envisioned as viable avenues to achieve this goal. Among them, one may mention trapped-ion arrangements and optical lattices as well as spin systems and quantum dots. While the list of such possibilities keeps increasing with time, quantum optics has so far provided a versatile platform where such ideas can be experimentally realized and tested. As indicated in recent studies, in optics, quantum information processing can be achieved entirely linearly, using simple passive components like beam splitters and phase shifters along with standard photodetectors and single-photon sources. In this same optical realm, quantum entanglement can arise as a natural byproduct of photon interactions-a clear manifestation of their particle-wave duality. Perhaps, nowhere this process is more apparent than in the so-called Hong-Ou-Mandel two-photon interference effect. In this latter configuration, photon entanglement is made possible via quantum interference-afforded after scattering from a beam-splitter. Lately, optical arrays of evanescently coupled waveguides have been suggested as a possible route toward the implementation of multiport systems with moldable quantum dynamics. The flexibility offered by such compact and often miniaturized optical NN configurations is made possible by the exceptional control achievable these days in microfabrication techniques. In this regard, Bloch oscillations of NOON and W

entangled states as well as quantum random walks have been considered in such arrays. In addition, the evolution of quantum correlations in both periodic and random (Anderson) lattices have also been investigated. The question naturally arises as to whether such multiport array systems can be utilized as a means to manipulate and engineer quantum states of light?. In other words can one exploit the multiple scattering events occurring in such structures as a means to build the required N-dimensional unitary transformation needed to synthesize and manipulate multipartite quantum states? In this chapter we investigate the propagation dynamics of non-classical light in a new class of dynamic photonic systems-the so-called Glauber-Fock oscillator lattices. We demonstrate that Bloch-like revivals and dynamic delocalization effects can naturally occur in spite of the fact that the structure itself is semi-infinite and not periodic. Interestingly, these interactions can be described in closed form, from where one can analytically deduce the turning points of these quantum oscillations. More importantly, the bunching and anti-bunching response of path-entangled biphotons can be pre-engineered in such coupled optical arrangements. Hypothetical Fermionic dynamics are also considered and compared to those expected from bosonic systems in these same arrays. Finally the possibility of experimentally realizing such Glauber-Fock oscillator lattices is discussed.

We begin our analysis by considering a semi-infinite array of evanescently coupled waveguides. In this arrangement the coupling coefficients among neighboring channels vary with the square root of the site index, i.e., $C_{k,k+1} \propto \sqrt{k+1}$. For generality,

we also allow this coupling to depend on the propagation distance in this lattice, in which case $C_{k,k+1} \propto f(Z)\sqrt{k+1}$, where $f(Z)$ is an arbitrary real function. In addition we also assume that the propagation constant (local eigenvalue) of each waveguide element varies linearly with the site position k. In essence, in this arrangement the refractive index is linearly increasing-in a way analogous to that of an externally biased crystal in solid state physics. Starting from these premises, one can show that in this class of arrays, the Heisenberg equation of motion for the creation operator is given by:

$$i\frac{da_k^\dagger}{dZ} - k\beta a_k^\dagger - \sqrt{k+1}\kappa a_{k-1}^\dagger - \sqrt{k}a_{k+1}^\dagger = 0, \tag{5.1}$$

In the above equation, represents a normalized propagation distance, and is a real constant associated with the strength of the aforementioned linear index change among successive sites. We emphasize that unlike standard infinite Bloch oscillator arrays [Kenkre, Morandotti, Lederer], the proposed structure is semi-infinite and asymmetric, e.g. the waveguides are no longer equidistant. As we will see later, these additional degrees of freedom may enable one to observe Bloch-like oscillations even in the neighborhood of the array boundary ($k = 0$). In general, the quantum dynamics in this Glauber-Fock oscillator array can be described through the evolution matrix $T(Z)$ that relates the input-output states, i.e.,

$$a_k^\dagger(0) = \sum_{n=0}^{\infty} T_{k,n}^*(Z) a_n^\dagger(0) \tag{5.2}$$

In (5.1), $T_{k,n}^*$ represents Hermitian conjugate of the element of this $\leftrightarrow T(Z)$ matrix or unitary transformation. We would like to emphasize that in the present case, the evolution matrix cannot be simply obtained from $\exp(-iHZ)$ since the Hamiltonian of the problem is Z (or time) dependent. Yet, in spite of this complexity, one can show that the evolution elements $T_{k,n}^*$ of this system can be obtained in closed form. These are given by:

$$\begin{aligned} T_{k,n}(Z) &= \sqrt{\frac{n!}{k!}} e^{A(Z)-i\lambda nZ} [B(Z)]^{k-n} L_n^{k-n}\left(|B(Z)|^2\right), \qquad for \qquad n \leq k \\ T_{k,n}(Z) &= \sqrt{\frac{k!}{n!}} e^{A(Z)-i\lambda kZ} [B(Z)]^{n-k} L_n^{n-k}\left(|B(Z)|^2\right), \qquad for \qquad n \geq k \end{aligned} \tag{5.3}$$

where in the above equations,

$$\begin{aligned} A(Z) &= -\int_0^Z \left(\int_0^{Z''} e^{i\lambda Z' - Z''} \right) f(Z'') dZ'', \\ B(Z) &= -i \int_0^Z e^{-i\lambda Z'} f(Z') dZ', \\ C(Z) &= -e^{-i\lambda Z} B^*(Z). \end{aligned} \tag{5.4}$$

In (5.4) L_n^m represent associated Laguerre polynomials. In order to gain insight into the quantum dynamics in this class of arrays, let us first consider the case where only a single photon is launched into the k-th waveguide element. We begin by analyzing here the simplest possible scenario where the Hamiltonian of the system

is Z-independent, thus $f(Z) = \gamma$ with γ is a real constant. Under these conditions, the evolution matrix elements are given by

$$T_{k,n}(Z) = \sqrt{\frac{n!}{k!}} e^{\delta - i\lambda n Z} \left[\frac{\gamma}{\lambda}\left(e^{-i\lambda Z} - 1\right)\right]^{k-n} L_n^{k-n}\left(\frac{2\gamma^2}{\lambda^2}\left(1 - \cos(\lambda Z)\right)\right), \qquad for \qquad n \leq k$$
$$T_{k,n}(Z) = \sqrt{\frac{k!}{n!}} e^{\delta - i\lambda k Z} \left[\frac{\gamma}{\lambda}\left(e^{-i\lambda Z} - 1\right)\right]^{n-k} L_n^{k-n}\left(\frac{2\gamma^2}{\lambda^2}\left(1 - \cos(\lambda Z)\right)\right), \qquad for \qquad n \geq k \tag{5.5}$$

where $\delta = i\gamma^2\lambda^{-1} + \gamma^2\left(e^{-i\lambda Z} - 1\right)\lambda^{-2}$. In this case the probability of finding this single-photon at waveguide site n when launched at k , can be obtained from $P_{n,k}(Z) = \langle a_n^\dagger a_n \rangle = |T_{k,n}|^2$. Eqs.(5.5) clearly indicate that the associated probability distribution exhibits revivals at regular intervals, e.g. at $Z = 2\pi s\lambda^{-1}$ (s being integer). At these revival points, for single-photon excitation, all the $T_{k,n}$ coefficients of Eq. (5.5) vanish except for , i.e., the probability collapses into the initial waveguide site k. Fig.5.1 depicts this process for such a Glauber-Fock oscillator array for different values of λ. These top views clearly show the previously mentioned "collapse" and revivals of the probability at $Z = 2\pi s\lambda^{-1}$ irrespective of the site where the photon was initially coupled. In all cases, those Bloch-like oscillations occur and the photon does not escape into the bulk region-towards the right. This in spite of the fact that the optical potential linearly increases and the waveguide elements get physically closer towards higher values of n. We note that unlike standard Bloch oscillations occurring in periodic lattices [xx], in this system the dynamics are asymmetric. This broken symmetry is a result of the semi-infinite nature of this

particular array.

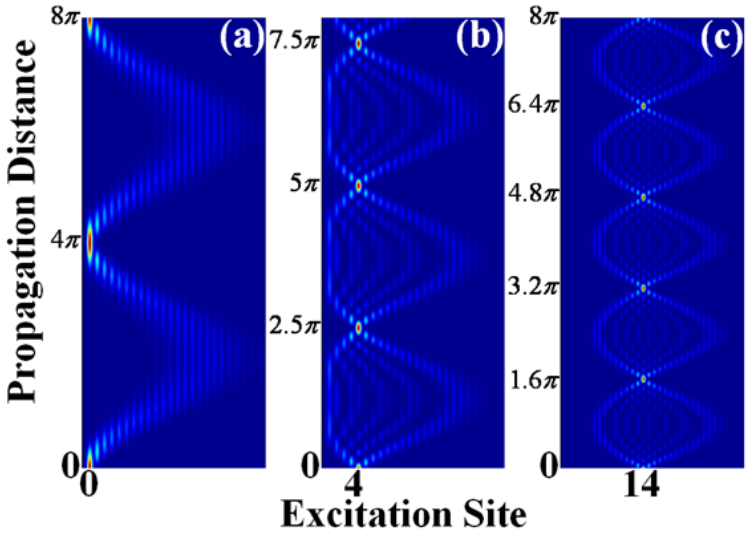

Figure 5.1: **Bloch-like oscillations for a single photon propagating in this class of arrays having 30 elements. The used lattice parameters are** $\gamma = 1$ **and (a)** $\lambda = 1/2$**, (b)** $\lambda = 4/5$**, and (c) 5/4. Note for all the cases collapse and revivals of probability occur at multiples of** $Z = 2\pi/\lambda$

We now focus our attention on the case where the coupling coefficients are Z-dependent, that is when the Glauber-Fock oscillator is dynamic. For illustration purposes we consider the periodic variation: $f(Z) = \kappa_0 + \varepsilon \cos(\varpi Z)$, where κ_0 is a constant, ε is a coupling modulation amplitude, and ϖ stands for the modulation frequency along the propagation direction. In this dynamic environment, when a single photon is launched into the k-site, the probability will periodically "collapse" into the initial waveguide, at exactly the first zero $\widehat{Z}$ of the function $|B(Z)|^2$. For

the particular example examined here these revivals occur the ratio $\varpi/\lambda = P/Q$ is a rational number where P, Q are relatively prime integers. This condition is necessary for the two oscillations occurring in this array (Bloch and from the coupling) to lock together synchronously. From here one can deduce that $\widehat{Z} = 2P\pi/\varpi$ This behavior is explicitly illustrated in Fig. 5.2 for $\kappa_0 = 1$, $\lambda = 1$, $\varepsilon = 0.2$ for the cases $\varpi = 1/2$, $2/3$, $3/4$ in (a), (b), and (c), respectively. The dashed lines on the other hand represent the evolution of the function which dictates the period of oscillations. Note that exact revivals do not occur if the ratio ϖ/λ is irrational.

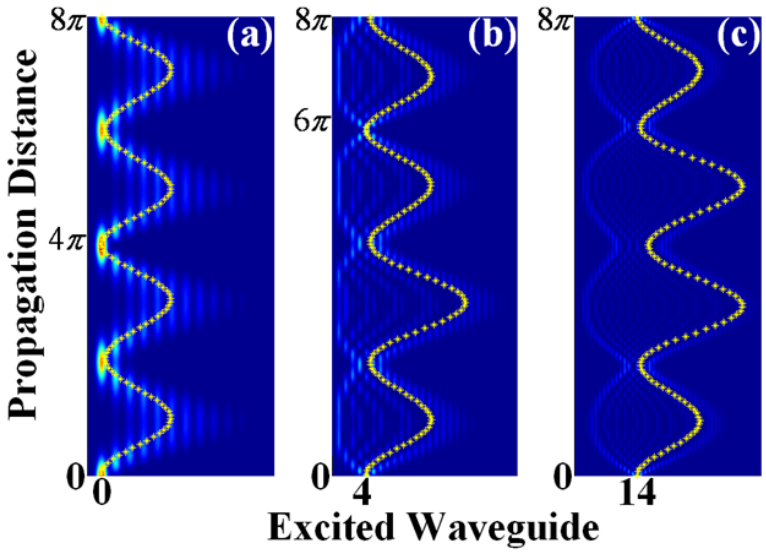

Figure 5.2: **response for three different lattices with $\lambda = 1$, and $\varpi = 1/2$, $2/3$, and $3/4$ for (a), (b) and (c) respectively. Dashed lines show the evolution of $|B(Z)|^2$ along giving the corresponding revival distance at $Z = 4\pi$, 6π, and 8π.**

On the other hand at resonance, $\varpi = \lambda$, *dynamic delocalization* occurs. In this regime $|B(Z)|^2 \propto Z$, and hence a drift motion is induced towards higher site indices. Therefore no pure oscillatory behavior is possible at resonance. This delocalization process around a resonance is depicted in Fig. 5.3. In this case, the probability of finding photon gradually shifts towards the right side of array oscillator.

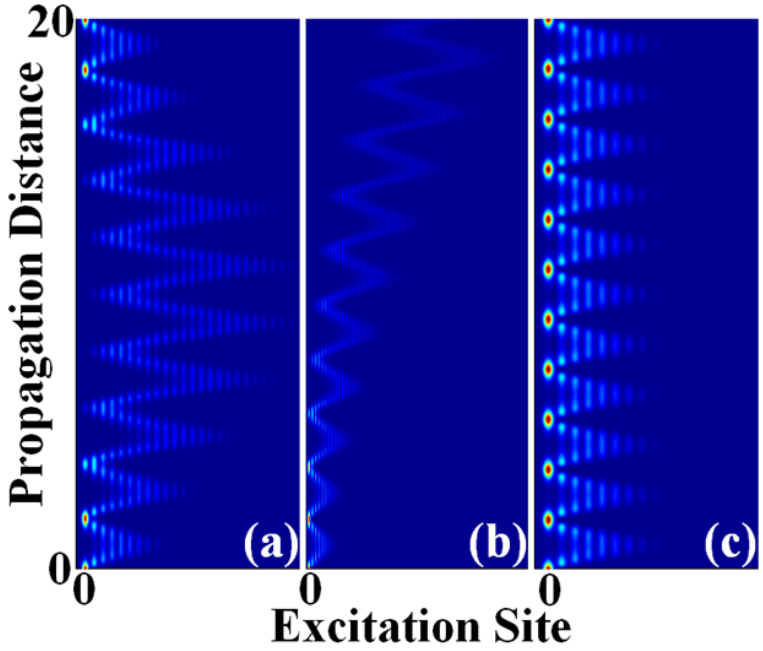

Figure 5.3: **Probability evolution corresponding to a single photon propagating through arrays of (a) 30, (b) 60, and (c) 30 waveguides.** $\lambda = 1$ **in all the cases, (a)** $\varpi = 0.9$**, (b)** $\varpi = 1$**, and (c)** $\varpi = 1.1$**.**

We next consider the quantum dynamics of an entangled pair of photons, launched either spatially correlated or anti-correlated positions in this class of Glauber-Fock oscillator arrays. As we will see, this class of systems can influence the bunching and

anti-bunching behavior of path-entangled biphotons. Conceptually, photon pairs (biphotons) with correlated positions will couple into the same waveguide (within a certain excitation window W) with an equal degree of probability. In this regime, the corresponding input state is written as

$$|\psi_C\rangle = \frac{1}{\sqrt{W}}\left[\left(a_f^\dagger\right)^2 + \left(a_{f+1}^\dagger\right)^2 + ... + \left(a_l^\dagger\right)^2\right]|0\rangle \tag{5.6}$$

Throughout our paper, f, and l will represent the first and last waveguide site within the excitation window. This input state can be generated by placing the waveguide array immediately after a type I collinear degenerate narrow-band spontaneous parametric down conversion (SPDC) thin-crystal source. On the other hand, an entangled pair of photons with anti-correlated positions corresponds to the physical situation where the photon pair is always coupled to waveguides on opposite sides of the excitation window W-again with equal probability. Thus, the input state is written as

$$|\psi_A\rangle = \frac{1}{\sqrt{W/2}}\left[a_f^\dagger a_l^\dagger + a_{f+1}^\dagger a_{l-1}^\dagger + ... + a_R^\dagger a_{R'}^\dagger\right]|0\rangle \tag{5.7}$$

where is even and represent the floor and ceiling integers of the quantity . In order to obtain the correlation between the array modes, we analyze at the output the coincidence rate at waveguides, which is given by $\Gamma_{p,q} \equiv \langle a_p^\dagger a_q^{gad} a_q a_p\rangle$. In this case one can show that for correlated inputs $|\psi_C\rangle$, the correlation map is

described by $\Gamma_{p,q} = \left|\sum_{k=f}^{l} T_{p,k}T_{q,k}\right|^2$, whereas for anti-correlated $|\psi_A\rangle$ it becomes $\Gamma_{p,q} = \frac{1}{2}\left|\sum_{k=0}^{W-1} T_{p,f+k}T_{q,l-k}\right|^2$. In order to demonstrate these effects and for comparison purposes, we will always here assume that with the excitation contained between.

Figure 5.4 depicts the evolution of the correlation map $\Gamma_{p,q}$ as a function of distance when $f(Z) = 1$ and $\lambda = 1/2$. In this case, revivals are expected at multiples of $Z = 4\pi$. When is initially correlated, the map flips and anti-bunching occurs at $Z = \pi$, and $Z = 3\pi$ while it returns to a broadened bunched state in the middle of a cycle. The situation changes when an anti-correlated biphoton input is used. In this case the map tends to flip over to that of a bunched state at $Z = \pi$, and $Z = 3\pi$ while in the middle of this oscillation it attains a correlation mixture-with bunching being predominant. This evolution is altogether different from that occurring in uniform lattices [x]. Here, the observed dynamics is a direct outcome of the revivals and of the phase acquired upon reflection from the boundary of this semi-infinite Glauber-Fock oscillator array. We next consider the evolution of correlations when two periods are simultaneously involved in the lattice, e.g. when the $f(Z)$ function is periodic. For this example we again take $f(Z) = \kappa_0 + \varepsilon\cos(\varpi Z)$ with $\kappa_0 = 1$, $\lambda = 1/2$, $\varepsilon = 0.2$ and $\varpi = 3/4$ in which case the period is 8π. For a correlated input $|\psi_C\rangle$ the correlation map approximately unfolds in the same as in Fig. 5.4(a)-(c) with twice the period. However at the half-cycle point the bunching is now not entirely complete. This scenario becomes very different when the initial biphoton state ψ_A

is anti-correlated. The correlation dynamics corresponding to this case is shown in Fig. 5.5 up to half a cycle 4π. Evidently, right after the origin, bunching is seen to occur Fig. 5.5(b) while midway in the cycle signatures of anti-bunching behavior appear. This latter pattern is different from that obtained before in Fig. 4(e) when only one oscillation frequency was governing the Glauber-Fock oscillator. We have also explored the response of this system under dynamic delocalization conditions. Figure 5.6 depicts again the correlations for the same parameters used in Fig.5.5, except that in this case $\lambda = \varpi = 1$. In this delocalization regime, a correlated input $|\psi_C\rangle$ tends to initially oscillate between bunching and anti-bunching Fig. 5.5(b) and eventually settles into anti-bunched state Fig.5.5(c). On the other hand, for an anti-correlated bi-photon input $|\psi_A\rangle$ the entangled photons very quickly and irreversibly become bunched and they remain in this state-Figs. 5.5(d)-(f). The reason delocalization affects the correlation evolution is because the photons tend to eventually escape into the bulk of lattice-away from the boundary. Simulations indicate that by adjusting the two oscillation frequencies one can at will lock the output into a particular bunching/anti-bunching state. In essence the presence of revivals (or absence of revivals) allows one to engineer the quantum dynamics in this class of dynamic Glauber-Fock oscillator lattices. Finally, we also consider this same arrangement when Fermionic input states are used. Figure 6 shows how the correlation evolves in this case under delocalization conditions for parameters identical to those used in Fig. 5. The input in this case is assumed to be of the

type $b_f^\dagger b_l^\dagger |0\rangle$. For this input, the anti-bunching behavior in the correlation matrix is clear. In conclusion we have shown that a new family of dynamic arrays, the so-called Glauber-Fock oscillator lattices can be used to mold the quantum evolution of path-entangled photons. In these systems revivals and dynamic delocalization are possible-each leaving a specific mark on the correlation map. If the two oscillation periods of these Bloch-like oscillators are irrational with respect to each other, the dynamics become aperiodic. In the future, of interest will be to examine how such structures respond to specific quantum states (like NOON states for example) or whether they can be used to synthesize other quantum states of interest. The response of these lattices may also be used to consider a similar class of problems in other array configurations that have quantum analogues like those of the Bose-Hubbard or Jaynes-Cummings type.

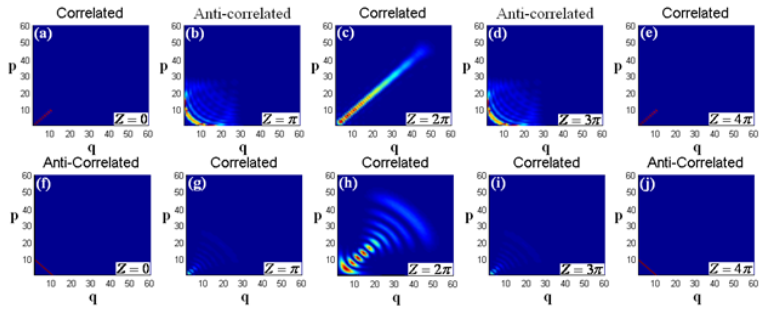

Figure 5.4: **Correlation maps corresponding to $|\psi_C\rangle$. (a, e) show the transition from the initial state with correlated through anti-correlated, correlated (magnified), anti-correlated, and correlated positions. (Bottom row) In contrast to $|\psi_C\rangle$, $|\psi_A\rangle$ suffers a transition from anti-correlated to a superposition of correlated and anti-correlated states.**

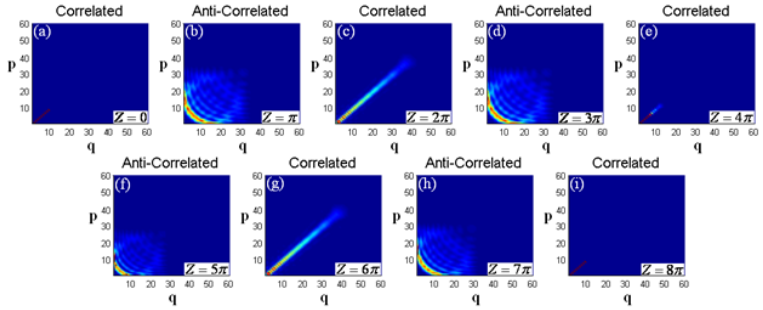

Figure 5.5: **Modulated and tilted Glauber-Fock oscillator array of 60 elements with $\lambda = 1$, $\varpi = 0.75$.**

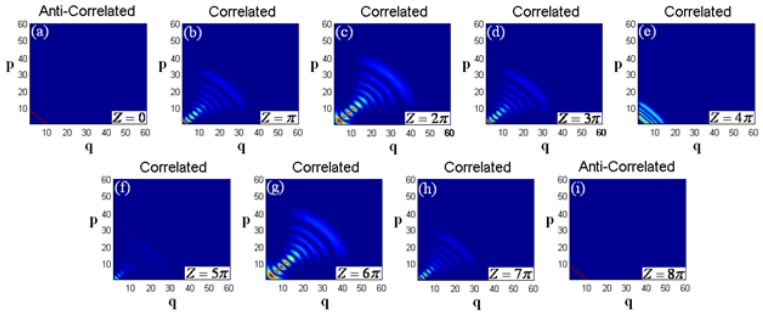

Figure 5.6: **Modulated and tilted Glauber-Fock oscillator array of 60 elements with $\lambda = 1$, $\varpi = 0.75$.**

Chapter 6

Conclusions

In chapter 3, we have shown that optical wave propagation in discrete photonic lattices having a square law distribution for the coupling coefficients effectively mimic quantum coherent, and displaced Fock states. This was done by judiciously adjusting the separation distance between identical waveguide elements, in such a manner that the coupling constants vary as $\sqrt{n}$. Analytical solutions in 1D topologies have been obtained. In addition, these prediction were experimentally corroborated by inscribing femtosecond (fs) laser waveguides in fused silica, so providing the required coupling distribution in a controlled fashion by only changing the distance between neighboring waveguides.

In chapter 4, we have shown that quantum correlation of indistinguishable particles in Glauber-Fock photonic lattices are unique for each input state. The correlations further show typical bosonic bunching behavior: on-diagonal peaks, corresponding

to a high probability of detecting both photons in the same output region. These correlation maps yielded to unexplored quantum random walks which exploit the additional complexity associated with the left boundary of these lattices.

In chapter 5, we have theoretically demonstrated the existence Bloch-like dynamics in semi-infinite non-periodic photonic, and Z-modulated potentials. Such localized waves can even exist at the boundary of the arrays. This counterintuitive phenomena was described analytically in terms of the generalized Laguerre polynomials.

Bibliography

[1] D. N. Christodoulides, F. Lederer, and Y. Silberberg, Nature 424, 817 (2203).

[2] Alberto Politi, Martin J. Cryan, John G. Rarity, Siyuan Yu, and Jeremy L. OBrien, Science 320, 5876 (2008).

[3] Andrei Faraon et al 2011 New J. Phys. 13 055025.

[4] Alex S. Clark, Jeremie Fulconis, John G. Rarity, William J. Wadsworth, and Jeremy L. O'Brien Phys. Rev. A 79, 030303(R) (2009)

[5] Anthony Laing, Terry Rudolph, and Jeremy L. O'Brien, Phys. Rev. Lett. 102, 160502 (2009).

[6] Jeremy L. O'Brien Science, 318, 1467 (2007).

[7] R. Akis, and D.K. Ferry, Appl. Phys. Lett. 79, 2823 (2001).

[8] U. Peschel, T. Pertsch, and F. Lederer, "Optical Bloch oscillations in waveguide arrays," Opt. Lett. 23, 1701-1703 (1998).

[9] T. Pertsch, P. Dannberg, W. Elflein, and A. Bruer, Phys. Rev. Lett. 83, 47524755 (1999).

[10] Henrike Trompeter, Thomas Pertsch, and Falk Lederer. Phys. Rev. Lett. 96, 023901 (2006).

[11] R. Iwanow, D. A. May-Arrioja, D. N. Christodoulides, and G. I. Stegeman, Phys. Rev. Lett. 95, 053902 (2005).

[12] Martin, Lane; Di Giuseppe, Giovanni; Perez-Leija, Armando; Keil, Robert; Dreisow, Felix; Heinrich, Matthias; Nolte, Stefan; Szameit, Alexander; Abouraddy, Ayman F; Christodoulides, Demetrios N; Saleh, Bahaa Optics Express, Vol. 19 Issue 14, pp.13636-13646 (2011)..

[13] Yoav Lahini, Assaf Avidan, Francesca Pozzi, Marc Sorel, Roberto Morandotti, Demetrios N. Christodoulides, and Yaron Silberberg Phys. Rev. Lett. 100, 013906 (2008).

[14] Tal Schwartz, Guy Bartal, Shmuel Fishman, and Mordechai Segev, Nature 446, 52-55 (2007).

[15] A. L. Jones, J. Opt. Soc. Am. 55, 261 (1965).

[16] S. Somekh, E. Garmire, A. Yariv, H. L. Garvin and R. G. Hunsperger, Appl. Phys. Lett. 22, 46 (1973).

[17] D. N. Christodoulides and R. I. Joseph, Opt. Lett. 13, 794 (1988).

[18] Y. Silberberg and G. I. Stegeman, J. Opt. Soc. Am. A 3 P41 (1986).

[19] W. K. Lai, V. Buek, and P. L. Knight, Phys. Rev. A 43, 63236336 (1991).

[20] Jonathan C. F. Matthews, Alberto Politi, Andr Stefanov, and Jeremy L. O'Brien, Nature Photonics 3, 346 - 350 (2009).

[21] H. F. Taylor and A. Yariv, "Guided Wave Optics," Proc. IEEE 62, 1044 (1974).

[22] Dietrich Marcuse, "Theory of Dielectric Optical Waveguides," (Academic Press, 1991)

[23] A. Yariv, "Coupled-mode theory for guided wave optics," IEEE J. Quantum Electron. 9, 919 (1973).

[24] A. Yariv, and Pochi Yeh, "Photonics: Optical Electronics in Modern Communications," The Oxford Series in Electrical and Computer Engineering, (2000).

[25] Katsunari Okamoto, "Fundamentals of Optical Waveguides," Academic Press, (2000).

[26] Allan W. Snyder, JOSA, Vol. 62, Issue 11, pp. 1267-1277 (1972).

[27] W. H. Louisell, Quantum and Statistical Properties of Radiation (Wiley, 1973).

[28] Y. Bromberg, Y. Lahini, R. Morandotti, and Y. Silberberg, Phys. Rev. Lett. 102, 253904 (2009).

[29] Z. Y. Ou and L. Mandel, Phys. Rev. Lett. 61, 50 (1988).

[30] R. J. Glauber, Phys. Rev. 131, 2766 (1963).

[31] F. A. M. de Oliveira, M. S. Kim, and P. L. Knight, Phys. Rev. A 41, 2645 (1990).

[32] M. Boiteux and A. Levelut, J. Phys. A 6, 589 (1973).

[33] L. G. Lutterbach and L. Davidovich, Phys. Rev. Lett.78, 2547 (1997);

[34] K. Banaszek and K. Wodkiewicz, Phys. Rev. Lett. 82, 2009 (1999).

[35] P. Bertet et al., Phys. Rev. Lett. 89, 200402 (2002).

[36] D. Leibfried et al., Phys. Rev. Lett. 77, 4281 (1996).

[37] P. Alsing, D.-S. Guo, and H. J. Carmichael, Phys. Rev. A 45, 5135 (1992).

[38] S. A. Podoshvedov and J. Kim, Phys. Rev. A 77, 032319 (2008).

[39] A. I. Lvovsky and S. A. Babichev, Phys. Rev. A 66, 011801 (2002).

[40] A. Perez-Leija, H. Moya-Cessa, A. Szameit, and D. N. Christodoulides, Opt. Lett. 35, 2409 (2010).

[41] "Classical analogue of displaced Fock states and quantum correlations in Glauber-Fock photonic lattices", submitted.

[42] Abramowitz and Stegun: Handbook of Mathematical Functions, (1972).

[43] G. Arfken, Mathematical Methods for Physicists(Academic, 1985).

[44] A. Szameit et al., Opt. Exp. 15, 1579 (2007).

[45] A. Szameit et al., Appl. Phys. Lett. 90, 241113 (2007).

[46] F. Dreisow et al., Phys. Rev. Lett. 102, 076802 (2009).

[47] J. W. Fleischer et al., Phys. Rev. Lett. 90, 023902 (2003).

[48] A. Peruzzo et al., Science 329, 1500 (2010).

[49] Y. Lahini, Y. Bromberg, D. N. Christodoulides, and Y. Silberberg, Phys. Rev. Lett. 105, 163905 (2010).

[50] Phys. Rev. Lett. 105, 263604 (2010).

[51] Phys. Rev. Lett. 85, 2733 (2000).

[52] T. Rom et al., Nature 444, 733 (2006); I. Bloch, J. Dalibard, and W. Zwerger, Rev. Mod. Phys. 80, 885 (2008).

[53] F. Bloch, Z. Phys. 52, 555, (1929).

[54] T. Pertsch, P. Dannberg, W. Elflein, and A. Bruer. Phys. Rev. Lett. 83, 47524755 (1999).

[55] R. Morandotti, U. Peschel, J. S. Aitchison, H. S. Eisenberg, and Y. Silberberg, Phys. Rev. Lett. 83, 4756 (1999)

[56] Y. Bromber, Y. Lahini, and Y. Silberberg, Phys. Rev. Lett. 105, 263604 (2010).

[57] R. El-Ganainy, D.N. Christodoulides, C. Ruter, and D. Kip, Optics Letters, Vol. 36 Issue 8, pp.1464-1466 (2011).

[58] U. Peschel, T. Pertsch, and F. Lederer, Optics Letters, Vol. 23 Issue 21, pp.1701-1703 (1998).